Trigeminal innervation and tactile responses in mouse tongue

Linghua Zhang[1], Maximilian Nagel[2], William P Olson[1], Alexander T. Chesler[2] and Daniel H. O'Connor[1]

[1]Solomon H. Snyder Department of Neuroscience, Krieger Mind/Brain Institute, Kavli Neuroscience Discovery Institute, The Johns Hopkins University School of Medicine, Baltimore, MD, USA.
[2]Sensory Cells and Circuits Section, National Center for Complementary and Integrative Health, Bethesda, MD, USA

The mammalian tongue is richly innervated with somatosensory, gustatory and motor fibers. These form the basis of many ethologically important functions such as eating, speaking and social grooming. Despite its high tactile acuity and sensitivity, the neural basis of tongue mechanosensation remains largely mysterious. Here we explored the organization of mechanosensory afferents in the tongue and found that each lingual papilla is innervated by Piezo2^{+} trigeminal neurons. Notably, each fungiform papilla contained highly specialized ring-like sensory neuron terminations that circumscribe the taste buds. Myelinated lingual afferents in the mouse lingual papillae did not form corpuscular sensory end organs but rather had only free nerve endings. *In vivo* single-unit recordings from the trigeminal ganglion revealed two types of lingual low-threshold mechanoreceptors (LTMRs) with conduction velocities in the Aδ range or above and distinct response properties: intermediately adapting (IA) units and rapidly adapting (RA) units. IA units were sensitive to static indentation and stroking, while RA units had a preference for tangential forces applied by stroking. Lingual LTMRs were not directly responsive to rapid cooling or chemicals that can induce astringent or numbing sensations. Genetic labeling of lingual afferents in the tongue revealed at least two types of nerve terminal patterns, involving dense innervation of individual fungiform papillae by multiple putatively distinct afferents, and relatively sparse innervation of filiform papillae. Together, our results indicate that fungiform papillae are mechanosensory structures, while suggesting a simple model that links the functional and anatomical properties of tactile sensory neurons in the tongue.

Introduction

The sense of touch is crucial for the function of the mammalian tongue in numerous behaviors including chewing (Pippi et al., 2018), swallowing (Chee et al., 2005; Tei et al., 2004), social grooming (Stern and Johnson, 1989) and vocalizing (Blom, 1960; Niemi et al., 2002). Unlike tactile information from the skin, tactile information from the tongue is often closely associated with chemo- and thermosensory inputs from food and drink, which together produce a vivid and complex mouthfeel. In terms of tactile acuity and sensitivity, the tip of the human tongue outperforms the fingertips with a lower two-point discrimination threshold and a lower mechanical threshold (Trulsson and Essick, 1997, 2010; Aktar et al., 2015; Miles et al., 2018). However, compared to other touch-sensitive organs including the hands/paws and the whiskers (Abraira and Ginty, 2013), the tongue has been less well characterized in terms of the sensory neuron subtypes and local architecture of nerve terminals underlying tactile sensitivity.

The dorsal surface of the tongue, which contacts food and drink, is covered with stratified squamous epithelium and contains four types of small protrusions called papillae: filiform, fungiform, circumvallate and foliate papillae, of which the filiform papillae and the fungiform papillae are the most abundant (Goździewska-Harłajczuk et al., 2018; Reginato et al., 2014) (**Figure 1**). On the mouse tongue, there are over 7000 conical-shaped filiform papillae that cover almost the entirety of the dorsal surface (Y. Wang et al., 2016). The less abundant, mushroom-shaped fungiform papillae host taste buds, and are concentrated at the tip and sides of the tongue. Based on their shape and abundance, filiform papillae have been hypothesized to be responsible for receiving tactile input (Böck, 1971; Kunze, 1969; Sato et al., 1988) and to act either as strain sensors or strain amplifiers (Lauga et al., 2016). However, the observation that sensory afferents expressing the mechanotransduction channel Piezo2 (Chesler et al., 2016; Ranade et al., 2014) can be found in both filiform and fungiform papillae (Moayedi et al., 2018), and that the density of fungiform papillae is positively correlated with lingual tactile sensitivity in humans (Bangcuyo and Simons, 2017; Essick et al., 2003; Yackinous and Guinard, 2001; Zhou et al., 2021), suggests that fungiform papillae may also be involved in touch sensation. Complicating the matter further, a group of fibers in the chorda tympani – a branch of the facial nerve that innervates taste buds within fungiform papillae and carries taste information – can also respond to stroking but not pressure on the tongue (Donnelly et al., 2022; Donnelly et al., 2018). Questions about how the filiform and fungiform papillae are innervated by somatosensory neurons from the trigeminal ganglion (TG), how lingual LTMRs respond to different tactile stimuli, and whether those nerve terminals form sensory end organs in the tongue, remain to be answered.

Here, we approached these questions using single-unit recordings from TG lingual LTMRs in anesthetized mice together with genetic labeling and tracing experiments. Our results uncover two groups of lingual LTMRs that differ in their tactile response properties, and suggest a model in which these two groups of LTMRs innervate different types of papillae and convey different information about touch on the tongue.

Results

Trigeminal ganglion projects to both filiform papillae and fungiform papillae in the mouse tongue

To investigate how papilla structures on the tongue are innervated by TG afferents, we labeled TG afferents in the anterograde direction in fixed mouse tissue by placing DiI crystals into the TG and examined the entire dorsal surface of the tongue. In neonatal mice (postnatal day (P) 0 and P10, n = 3, respectively), the tip of the tongue had the highest innervation density (**Figure 2A**). Filiform papillae were innervated by DiI-labeled TG afferents (**Figure 2B**, arrows; **Figure 2C**), including those at the anterior part of the tongue and those inside the intermolar eminence (**Figure 2A**, arrows). Surprisingly, not only the filiform papillae, but also the fungiform papillae were strongly labeled by TG afferents from anterior to posterior (**Figure 2A** and **2B**, triangles; **Figure 2D**). In contrast, previous studies suggest that the chorda tympani afferents from the geniculate ganglion (GG), which consist of gustatory fibers primarily and a subset of thermo- or mechanosensory fibers (Yokota and Bradley, 2016; Donnelly et al., 2018), only innervate fungiform papillae (Fei et al., 2014). Together, these findings suggest that the innervation pattern of TG afferents differs from that of GG afferents, and that both types of lingual papillae may be involved in somatosensation (**Figure 2E**).

Trigeminal afferents innervate the extragemmal region of fungiform papillae and exhibit a ring-like termination pattern surrounding the taste pore

The cross-section view of a fungiform papilla in **Figure 2D** shows that trigeminal afferents in a fungiform papilla penetrated the apical epithelium surrounding the taste pore and terminated in the extragemmal (outside of taste buds) region. To further explore the terminal organization of trigeminal afferents in fungiform papillae, we performed DiI anterograde tracing from the TG and examined fungiform papillae (n = 15) in confocal z-stacks, in order to better appreciate how the axons traveled through the papillae. Interestingly, we found that the trigeminal fibers exhibit a ring-like termination pattern in fungiform papillae in maximal intensity projections of the confocal stacks (**Figure 3A**), with little DiI signal in the middle part of the papillae where taste pores and taste buds were located. We found that the trigeminal nerve fascicles innervating a fungiform papilla met at the base of the connective tissue and entered the connective tissue core through the middle as a bundle (**Figure 3B**, sections 1–3; **Video S1**). The nerve bundle then bifurcated into multiple branches, traveled towards the side walls of the papilla and avoided the taste bud (**Figure 3B**, sections 4–7), while still going upwards beyond the level of the taste bud until reaching the apical epithelium surrounding the taste pore, forming a ring-shaped terminal organization (**Figure 3B**, sections 8). This finding is consistent with the description of the trigeminal innervation pattern in fungiform papillae in Suemune et al. (1992). The fact that the TG afferents innervating fungiform papillae are terminated at the superficial epithelium suggests that they are capable of detecting sensory stimuli, including mechanical stimuli, in an extremely sensitive manner.

To investigate the innervation pattern of mechanosensitive afferents expressing Piezo2, we examined the dorsal surface of the tongue in *Piezo2-EGFP-IRES-Cre/+;Snap25*$^{LSL\text{-}EGFP/+}$ mice

aged P1–P2 (n = 4) and *Piezo2-EGFP-IRES-Cre/+* mice injected with AAV9-pCAG-FLEX-tdTomato virus intraperitoneally at ages P1–P2 (n = 4) to avoid lineage problems caused by embryonic expression of Piezo2. As with DiI-labeled trigeminal afferents, fluorescently-labeled Piezo2^{+} afferents were found in both fungiform and filiform papillae but not their *Piezo2-EGFP-IRES-Cre/+;Snap25*$^{+/+}$ littermates (**Figure 3C**), suggesting that both types of papillae are involved in mechanosensation. Afferents expressing Piezo2 in fungiform papillae also exhibit a ring-like termination pattern (**Figure 3D,** white arrows). The side view of a fungiform papilla shows that Piezo2^{+} afferents innervated the extragemmal region rather than the intragemmal (inside taste buds) region (**Figure 3D**, yellow arrow; cf. **Figure 4D**, bottom row, arrowhead), similar to DiI-labeled trigeminal afferents (**Figure 2D**). Considering that GG afferents are not the major contributor to extragemmal afferents in fungiform papillae (Donnelly et al., 2022; Ohman-Gault et al., 2017), our results suggest that TG afferents are the main mechanosensory supply for fungiform papillae.

Mouse filiform papillae contain NFH^{+} myelinated free nerve endings without sensory end organs, while ferret filiform papillae contain corpuscular end organs resembling end bulbs of Krause

Sensory end organs are specialized structures formed at the terminals of sensory afferents that can act as mechanical filters and thus affect the mechanosensory responses of the axons. We next sought to describe any sensory end organs in the mouse tongue, with a special focus on the filiform papillae, where sensory innervation is solely provided by trigeminal afferents.

We found that both filiform papillae and fungiform papillae in the mouse tongue are innervated by NFH^{+} myelinated afferents, consistent with prior work (Moayedi et al., 2018; Sato et al., 1988) (**Figure 4A and S1**). In order to visualize the shape of terminal Schwann cells, which are often involved in the structure of sensory end organs, we used both immunostaining (S100β) and genetic labeling (*Plp1-EGFP*) methods targeting terminal Schwann cells. In contrast to the glabrous skin, where we easily identified corpuscular end organs such as Meissner corpuscles by immunostaining S100β or genetically labeling PLP1 (**Figure 4A**, lower panels), we could not find corpuscular end organs (e.g. structures resembling end bulbs of Krause or Meissner corpuscles in shape) in the filiform papillae of the mouse tongue (**Figure 4A**, upper panels). The lack of Merkel cells at the apical epithelium of tongue reported by other research groups (Donnelly et al., 2022; Moayedi et al., 2018) also suggests that the nerve terminals ascending the connective tissue cores of papillae were not likely to be associated with Merkel cells.

By conducting a small-scale screen of Cre mouse lines (Table 1), we identified several Cre lines that can label neuronal afferents on the surface of the tongue, including *Pirt*^{Cre}, *Vglut2*^{Cre} and *Split*^{Cre}, which allowed us to better visualize the afferent terminals with genetic labeling strategies. In both *Pirt*^{Cre}*;Plp1-EGFP;R26*$^{LSL\text{-}tdTomato}$ mice and *Vglut2*^{Cre}*;Plp1-EGFP;R26*$^{LSL\text{-}tdTomato}$ mice, tdTomato-labeled, myelinated as well as unmyelinated primary afferents can be found in both fungiform papillae and filiform papillae. The terminal Schwann cells in mouse filiform papillae did not arrange in a compact stack and form either oval or cylindrical structures overall

as in sensory corpuscles; rather, they merely formed a myelin sheath, which went missing before reaching the terminations of lingual afferents, leaving the nerve endings free (**Figure 4B** and **4C**, triangles). In fungiform papillae, *Vglut2*^{Cre} labeled at least two different groups of afferents defined by their terminal locations: the intragemmal afferents innervating the taste bud (**Figure 4C**, arrowhead), and the extragemmal afferents that penetrated the apical epithelium surrounding the taste pore (**Figure 4C**, thick arrows). The terminals of both fungiform groups also did not associate with any PLP1-EGFP^{+} corpuscular structures. In *Split*^{Cre}*;Plp1-EGFP;R26*$^{LSL\text{-}tdTomato}$ mice, tdTomato-labeled unmyelinated primary afferents with free nerve endings were found in both fungiform papillae and filiform papillae (**Figure 4D**, arrows), which may represent nociceptors with lower conduction velocities.

The average size and the shape of tongue filiform papillae vary across mammalian species, as do their degrees of keratinization and their structural complexity. Previous studies have identified the existence of a type of simple corpuscle through immunohistochemistry and electron microscopy in the more developed filiform papillae of cats and cattle (Sato et al., 1988; Spassova, 1974), but not in the smaller and simpler filiform papillae of rats (Sato et al., 1988). To provide comparative context and test our ability to identify lingual end organs, we examined nervous elements in the ferret tongue by immunostaining myelinated afferents (NFH) and terminal Schwann cells (S100β). We found that the majority of nerve afferents in the ferret tongue were not associated with corpuscles. However, unlike in the mouse tongue, ferret filiform papillae contained end organ structures with varied shapes, including cylindrical or globular structures that resembled the simple end bulbs of Krause in cats (**Figure 4E**, top and middle panels). Individual filiform papillae could contain more than one end organ (**Figure 4E**, bottom panel). Moreover, the lingual afferents encapsulated in a corpuscle usually had enlarged, blunt nerve endings (**Figure 4E**, all three panels), and could branch at the terminal (**Figure 4E**, bottom panel). Collectively, these results demonstrate that our methods allow us to identify sensory end organs, highlight structural differences among filiform papillae of different animal species, and show that those of the mouse lack obvious sensory end organs.

Single-unit recordings reveal two types of lingual LTMRs with distinct tactile response properties and conduction velocities in the A-fiber range

By injecting DiI into either the tip of the tongue or the left whisker pad in different groups of mice (n = 3 for each), we found that TG neurons innervating the tip of the tongue had their cell bodies mostly located near or at the ventral side of the mandibular branch of TG, as compared to whisker pad-innervating neurons, whose cell bodies can be found at both dorsal and ventral sides of the TG (**Figure S2**). To investigate the tactile properties of lingual LTMRs, we performed single-unit recordings with tungsten electrodes in the TG of anesthetized mice. After anesthesia, the tongue was carefully pulled out of the mouth using blunt forceps and placed on a surface that had a stable slope of 30 degrees from the vertical and against which the lower teeth were braced to keep the mouth open during recordings (**Figure 5A**). The surface of the tongue was gently stimulated using a fine-tip brush until the activity of a unit that was responsive to brush strokes was captured by the electrode in the TG. The stable platform setup prevented tongue stimulation from causing unintended, correlated movements of the jaw and the lower

chin as well as any potential mechanical stimulation of facial hairs on the lower face, which could lead to spurious inclusion of non-tongue units.

Using von Frey filaments to apply a constant force on their receptive fields (RFs), we found two types of lingual LTMRs that differed in their adaptation properties: an intermediately adapting (IA) type and a rapidly adapting (RA) type. The RA-LTMRs only fired at the onsets and offsets of the von Frey stimulation, whereas the IA-LTMRs fired at the onsets and offsets of applied force as well as during a short period of time after the applied force became stable (**Figure 5B**). The majority of both types of LTMRs had small RFs (less than 0.1 mm^2), and most IA-LTMRs recorded had their RFs located within 0.5 mm of the tip of the tongue (11 out of 19, or 57.9% IA units, **Figure 5C**), resembling the distribution of taste buds (cf. **Figure 1A and 2A**). Unlike GG mechanoreceptors innervating the tongue, which only respond to moving but not to static pressure (Donnelly et al., 2018), both types of TG lingual LTMRs had very low thresholds for static indentation, often less than 1.6 mN. Four out of five RA-LTMRs had von Frey thresholds higher than the IA-LTMRs, whose thresholds were always below 0.4 mN (**Figure 5D**) and could be as low as 0.2 mN (5 units) or 0.08 mN (1 unit, data not shown).

To measure the conduction velocity of lingual LTMRs, we first estimated the distance between the anterior part of the tongue to the TG through lingual nerve dissection and DiI tracing. By exposing the lingual nerve posterior to its exit from the tongue and cutting the nerve anterior to its entrance at the foramen ovale, we estimated the upper bound of the distance from the anterior part of the tongue to the TG in adult mice to be 1.8 cm. By injecting DiI at the tip of the tongue in live mice and using the known DiI traveling speed *in vivo* (6 mm/day; Godement et al., 1987; Honig and Hume, 1986), we estimated the lower bound of the distance from the anterior part of the tongue to the TG in adult mice to be 1.1 cm. These distances are short enough to limit proper measurement of fast axonal conduction velocity due to potential masking by electrical artifacts of the first induced neuronal spike during stimulation. Hence, we could only estimate the conduction velocity of lingual IA- and RA-LTMRs as falling into the range of Aδ fibers (lower bound: 6.1 ± 2.7 m/s, higher bound: 9.9 ± 4.5 m/s; n = 4. **Figure 5E**) or above.

We also found that IA- and RA-LTMRs had distinct tactile preferences. Besides their high sensitivity to brush stroking (data not shown), IA-LTMRs were also highly sensitive to vertical forces as indicated by their extremely low von Frey thresholds. Their firing rates in an initial time period after the force onset increased as the static forces being applied increased (**Figure 5F**). When indented by a hand-held brush, where in contrast to the von Frey filaments the applied force is not constant, they fired during the entire period of stimulation (**Figure 5G**). This suggests that the IA-LTMRs are very sensitive to slight force changes in the vertical direction. In comparison, RA-LTMRs still fired only at the onsets and offsets of the indentation even with the hand-held brush (**Figure 5G**). They were highly responsive to brush stroking across their receptive fields. They were also sensitive to rapid changes of the buckling direction of von Frey filaments during indentation, even when the von Frey filaments used were below their von Frey thresholds for static indentation (**Figure 5G**). These observations suggest that RA-LTMRs were more sensitive to shear/tangential forces than to vertical forces.

As Pirt and Vglut2 were reported markers for geniculate ganglion neurons and primary sensory neurons including non-LTMR cell types in both trigeminal and dorsal root ganglion (Kim et al., 2008, 2016, 2015; Lagerström et al., 2010; Leijon et al., 2019; Patel et al., 2011; Vandenbeuch et al., 2010; Wu et al., 2015), we tested whether the neuronal afferents labeled by *Pirt*^{Cre} or *Vglut2*^{Cre} on the surface of the tongue partly originated from TG and included LTMR afferents. We performed single-unit recordings in the TG of *Pirt*^{Cre}*;R26*$^{LSL\text{-}ChR2}$ mice and *Vglut2*^{Cre}*;R26*$^{LSL\text{-}ChR2}$ mice, and recorded the responses of lingual LTMRs when their receptive fields were stimulated by 473 nm blue light (**Figure 5H**). 83% of lingual LTMRs in *Pirt*^{Cre}*;R26*$^{LSL\text{-}ChR2}$ mice (7 IA-LTMRs and 1 RA-LTMR from 3 mice; **Figure 5I**) and 100% of lingual LTMRs in *Vglut2*^{Cre}*;R26*$^{LSL\text{-}ChR2}$ mice (10 IA-LTMRs and 3 RA-LTMRs from 8 mice; **Figure 5J**) could be activated by blue light, suggesting that besides labeling GG neurons, *Pirt*^{Cre} and *Vglut2*^{Cre} can label lingual LTMRs in TG as well. Together, our results report that *Pirt*^{Cre} and *Vglut2*^{Cre} can label myelinated lingual afferents whose cell bodies are located in the TG, and that *Vglut2*^{Cre} can label for both lingual IA- and RA-LTMRs.

Lingual neurons that terminate in different types of papillae form distinct terminal fields

To investigate the terminal field patterns of lingual neurons in TG, we injected AAVPHP.S-CAG-FLEX-tdTom virus into the TG in *Vglut2*^{Cre} mice (n = 1), which allowed us to label a subset of mandibular branch neurons including lingual IA- and RA-LTMRs (**Figure 6A**). We found that the fungiform papillae from the anterior to the posterior part of the tongue were heavily labeled by tdTomato, with the tip of the tongue having the highest labeling density (**Figure 6B**). Moreover, tens of nerve terminals could be seen in a single fungiform papilla (**Figure 6C**), suggesting that there may be a large number of TG afferents innervating a single fungiform papilla even though axon branching may occur near the terminal. Occasionally, we could find weak tdTomato signals in several adjacent filiform papillae (~16 papillae) but not their neighbors (**Figure 6D**), pointing towards the possibility that the afferent terminals in the small filiform papillae cluster came from a single TG neuron whose axon branched and terminated into each papilla. A single filiform papilla, however, can be innervated by multiple TG afferents as shown in **Figure 4C-E**. These results suggest that lingual neurons in TG innervate different types of papillae and may form distinct terminal fields, and that the fungiform papillae have a more redundant trigeminal innervation compared with filiform papillae. The tip of the tongue, where fungiform papillae have the highest density, is thus equipped with the most somatosensory afferents from TG.

Lingual LTMRs are insensitive to rapid cooling or chemicals that can induce astringent or numbing sensations

The mammalian tongue is a sensory surface where mechanosensation, thermosensation and chemosensation closely interact with each other. Our daily experience of eating and drinking reminds us that the perception of food texture can be affected by the food temperature (Engelen et al., 2003). Also, there are some interesting types of tactile perception that can be induced by certain chemicals in food, such as the sense of astringency caused by chemicals containing the galloyl groups, including tannic acid in green tea, red wine and unripe fruits (Schöbel et al., 2014), and the sense of numbing induced by hydroxy-alpha-sanshool in green Sichuan

peppercorns harvested from *Zanthoxylum* species (Luo et al., 2022). We tested whether lingual LTMRs can be directly activated by temperature changes and certain chemicals applied on their RFs (**Figure 7A**). We did not observe responses to rapid cooling among a sample of lingual LTMRs (7 IA-LTMRs and 1 RA-LTMR from 6 mice, **Figure 7B**), consistent with prior findings on the thermal responses of lingual Aδ and Aβ mechanoreceptors in rats (Wang et al., 1993). Moreover, we did not observe responses to chemicals containing the galloyl groups in a series of concentrations, including 100 uM, 200 uM, 500 uM, 1000 uM tannic acid or EGCG applied on the tongue surface (5 IA-LTMRs and 1 RA-LTMR from 5 mice, **Figure 7C**). Although hydroxy-alpha-sanshool was shown to be able to interfere with the vibration detecting ability of RA channels on the fingertip (Kuroki et al., 2016), we did not find obvious differences in the mean firing rates of lingual RA-LTMRs measured before and after the application of 1300 uM hydroxy-alpha-sanshool (3 units from 2 mice, **Figure 7D**). RA-LTMRs also did not respond to the application of a commercial Kava concentrate drink on their RFs (3 units from 2 mice, **Figure 7E**). This drink contains extracts from the roots of *Piper methysticum* and induces numbing sensations on the human tongue within tens of seconds. Collectively, these results suggest that lingual LTMRs in mice cannot be directly stimulated at the nerve terminals by rapid cooling or certain chemicals that produce astringent or numbing sensations in humans, and are therefore likely unimodal touch sensors.

Discussion

In this study, we combined neuronal tracing, genetic labeling and single-unit recording methods to investigate the innervation of the tongue by trigeminal afferents and the response properties of different types of LTMRs in the tongue. We discovered broad innervation of both filiform and fungiform papilla types by TG afferents, and provide evidence that the lingual afferents in the mouse filiform papillae have myelinated free nerve endings. Lingual LTMRs in TG were classified into two types based on their adaptation properties: IA and RA. IA-LTMRs and RA-LTMRs had similarly small RFs and comparable conduction velocities in the A-fiber range, but differed in tactile preferences. Viral labeling revealed at least two types of terminal fields for TG afferents in the tongue with unique innervation patterns. Together, these results suggest a simple model that relates physiologically defined lingual LTMRs to anatomically defined patterns of innervation in the dorsal tongue (**Figure 8**).

A model for tactile innervation of the tongue

On average, the dorsal surface of the mouse tongue contains more than 7,000 filiform papillae and over 130 fungiform papillae in total (Y. Wang et al., 2016; Zhang et al., 2008). The number of TG neurons in mice, however, is around 50,000 at E13.5 (Wilkinson et al., 1996). Considering that the tongue is innervated by only a subset of the mandibular branch neurons in the TG, we drew the conclusion that the number of TG neurons innervating the tongue may be on the same order of magnitude as that of filiform papillae. We also learned, from the viral labeling experiments, that the fungiform papillae were significantly more heavily innervated by Vglut2^{+} TG neurons than the filiform papillae. How does the biological system assign the limited number of TG neurons to innervate such abundant filiform papillae and the much fewer fungiform

papillae, while assuring the heavy innervation of fungiform papillae? We propose, from the evidence we have gotten so far, that one TG neuron may branch at a region near the nerve terminal and innervate many adjacent filiform papillae at the same time, and that one fungiform papilla may be innervated by multiple TG neurons that do not branch to innervate nearby fungiform papillae. A single filiform papilla may also contain afferents from several TG neurons. Roughly, the innervation scheme may be [$N > 10^1$ or 10^2] TG neurons: 1 fungiform papilla, and [$N > 10^0$ or 10^1] TG neurons: [$N \approx 16$] adjacent filiform papillae.

Our single-unit recordings suggest that most lingual LTMRs have a very small RF, usually less than 0.1 mm^2. This is consistent with the size of the axon terminal fields of Vglut2$^+$ TG lingual neurons we observed in viral labeling. We note however that two units in our sample had apparently elongated RFs that included portions of the edge of the tongue (**Figure 5C**). The mapping for these RFs was likely imprecise, as the RFs may have extended to regions on the ventral tongue, which we did not explore and which could be indirectly stimulated by touching adjacent areas.

Our observation that lingual LTMRs can be grouped into two types based on adaptation properties, and our observation of two types of axon terminal fields among Vglut2$^+$ or myelinated TG lingual neurons, raises the question of whether the two physiological and two anatomical groups map onto one another. We consider it highly probable based on the following four points.
1. Optotagging of LTMRs confirmed that Vglut2 is a marker for both IA- and RA-LTMRs (**Figure 5J**). Therefore, by viral labeling Vglut2$^+$ lingual neurons in TG, we expected to see both IA- and RA-LTMRs' afferent terminals being labeled. In fact, we found two types of terminal field patterns (**Figure 6C** and **6D**), and it is likely that these may represent different types of Vglut2$^+$ lingual LTMRs, i.e. IA- and RA-LTMRs.
2. The different tactile properties of IA- and RA-LTMRs echoed the discrepancy of tissue properties of different papillae. IA-LTMRs generally had lower von Frey thresholds than RA-LTMRs and were sensitive to light indentation, while RA-LTMRs were sensitive to brush stroking, or in other words, tangential forces. Considering that the fungiform papillae are covered by a thin layer of keratinized pore cells and are non-keratinized at the taste pore region, whereas the filiform papillae consist of keratinized epithelium with higher tissue stiffness (Goździewska-Harłajczuk et al., 2018; Iwasaki et al., 1999; Okubo et al., 2009; B. Wang et al., 2016), we speculate that lingual IA-LTMRs that are sensitive to light forces in the vertical direction innervate the fungiform papillae, whereas lingual RA-LTMRs sensitive to tangential forces innervate the filiform papillae.
3. The relative abundance of IA- and RA-LTMRs found in recordings matched the uneven viral labeling of fungiform and filiform papillae. We encountered IA-LTMRs far more frequently than RA-LTMRs in our single-unit recordings. Similarly, in the viral labeling experiment where only a subset of Vglut2$^+$ TG neurons were labeled, labeled neurons terminating in fungiform papillae were far more abundant than those terminating in filiform papillae.
4. The locations of IA-LTMRs' RFs were highly similar to those of fungiform papillae. Most IA-LTMRs we recorded had their RFs located near the tip of the tongue (**Figure 5C**), where fungiform papillae are most abundant (**Figure 2A**). Moreover, some IA-LTMRs' RFs were

located along the midline of the tongue, mimicking the distribution pattern of fungiform papillae. Although our sample of RA-LTMRs was relatively small, this pattern was not evident.

The model depicted in **Figure 8** explains our observations, but will require more direct evidence. This could be obtained, e.g., by physiological characterization of individual LTMRs using juxtacellular recordings in the TG, followed by electroporation with an intracellular dye and *post hoc* anatomical reconstructions. Alternatively, genetic markers yet to be identified may in the future allow distinguishing IA- and RA-LTMRs using optotagged extracellular recordings combined with anatomical mapping.

Possible underlying mechanisms that endow the mouse tongue with high tactile sensitivity

We identified A-LTMRs with free nerve endings in the lingual mucosa that were not associated with sensory end organ structures akin to any known type, and yet which had small RFs and high tactile sensitivity. These lingual LTMRs presumably support fine discriminative touch for the tongue, yet differ markedly from Aβ-, Aδ- and C-LTMRs that support discriminative touch in the glabrous or hairy skin and that have specialized end-organ or hair-follicle terminations (Abraira and Ginty, 2013). We may speculate that the fungiform papillae, though classically considered gustation-related structures, may also serve in an end-organ role for touch.

Our study reveals an important role for fungiform papillae in touch sensation on the tongue, and provides an explanation as to why the tip of the tongue has the highest tactile sensitivity compared to other tongue regions. Previous studies either assumed that the filiform papillae are the primary mechanosensory organs of the tongue (Lauga et al., 2016), or focused on the mechanosensory afferents in chorda tympani innervating the fungiform papillae, which only respond to stroking but not to static tactile stimuli (Donnelly et al., 2018). A recent study in humans identified the existence of a type of sensory end organ whose morphology resembles that of Meissner corpuscle, a mechanosensory end organ responsible for detecting low frequency (below 300 Hz) vibrations (Mountcastle et al., 1967) in fungiform papillae, suggesting that the fungiform papillae are not merely a hub for gustatory machineries. Here, we supply a missing piece of the puzzle on mechanosensory mechanisms of the tongue by showing that the lingual LTMRs in the trigeminal ganglion are extremely sensitive to static forces, and that the fungiform papillae are heavily innervated by trigeminal afferents and Piezo2^{+} afferents. The high resemblance between IA-LTMR receptive field locations and fungiform papillae locations also indicates that the fungiform papillae contain mechanosensory afferents from the trigeminal ganglion and play an important role in tongue mechanosensation. This also explains the high tactile sensitivity at the tip of the tongue, considering that the tip of the tongue has the highest density of fungiform papillae and thus the highest mechanosensory innervation on the entire dorsal surface of the tongue (**Figure 2A**).

Previous studies show that GG neurons that can be labeled by the transcription factor Phox2b mainly terminate at the taste bud itself and make contact with taste bud cells, forming intragemmal projections (Ohman-Gault et al., 2017; Tang and Pierchala, 2022). A few

Phox2b-positive afferents were also seen to innervate the extragemmal region of fungiform papillae. Those were hypothesized to be mechanosensitive chorda tympani fibers as they were preserved together with the mechanosensitivity of chorda tympani fibers after taste bud elimination via inhibition of the Hedgehog signaling pathway (Donnelly et al., 2022). However, most of the extragemmal afferents in fungiform papillae were not Phox2b-positive, and Phox2b-positive extragemmal afferents were only seen in 43% of the fungiform papillae (Ohman-Gault et al., 2017), suggesting that the extragemmal afferents in fungiform papillae may have a main source other than the GG. We observed that unlike the termination pattern of the GG, the TG afferents terminate at the Piezo2$^+$ afferents-enriched extragemmal region of fungiform papillae, which suggests that the majority of the extragemmal mechanosensory afferents have a trigeminal origin. This is consistent with previous findings showing that the chorda tympani denervation had negligible effect on the extragemmal afferents (Whitehead et al., 1985).

In summary, TG afferents have a largely different innervation pattern compared to GG afferents. First, TG afferents provide somatosensory innervation to the filiform papillae, which are not supplied by GG afferents. Second, the termination patterns of TG and GG afferents in the fungiform papillae are largely non-overlapping. The TG nerve terminals occupy the Piezo2$^+$ afferents-enriched extragemmal space in the apical epithelium, while the majority of GG nerve terminals reside in the intragemmal space, with a few putatively mechanosensitive exceptions. This suggests a functional specialization in the nerve fibers innervating different regions of the fungiform papillae.

Modality specificity of lingual LTMRs

Previous work has shown that cutaneous C- and Aδ-LTMRs can be stimulated by rapid cooling of the skin (Li et al., 2011). A recent study using *in vivo* calcium imaging of mouse trigeminal neurons also identified lingual mechanosensory neurons that were responsive to a cooling stimulus applied to the tongue surface (Moayedi et al., 2023). Here we recorded from what appears to be a different population of lingual mechanosensory neurons. In particular, our sample of lingual LTMRs was insensitive to cooling on the tongue surface, consistent with previous findings showing that both Aδ and Aβ lingual mechanoreceptors in rats are specialized touch sensors with no response to either cold or warm stimuli (8–51 ℃) or menthol (Wang, 1993). This can be explained by the lack of Trpm8 (involved in cooling sensation; Bautista et al., 2007) expression in the vast majority of Piezo2$^+$ trigeminal neurons revealed by single-cell RNA sequencing and *in situ* hybridization (von Buchholtz et al., 2021; Nguyen et al., 2017), and lack of mechanical responses in Trpm8-expressing trigeminal neurons (von Buchholtz et al., 2021).

Our sample of tongue LTMRs was not directly stimulated by chemicals that induce astringent or numbing sensations. However, previous work found that some TG neurons can be activated by astringent compounds including tannic acid or EGCG *in vitro* (Schöbel et al., 2014). We think these neurons might be chemosensory or polymodal neurons in TG, and that it is worthwhile to perform *in vitro* chemical tests on Piezo2-expressing TG neurons.

Limitations of the study and future directions

Although we did not find sensory end organs resembling any known type at the dorsal surface of the mouse tongue, the lingual LTMRs may still be associated with structures that we have not yet examined at their terminals, such as collagen fibers. The potential association of lingual nerve terminals with collagen fibers may also affect their tactile response properties. Therefore, it is worthwhile to study the termination of lingual nerves through careful electron microscopy analysis.

Our model of tongue mechanosensation proposes that IA-LTMRs innervate the fungiform papillae. This can be directly tested by stimulating a single fungiform papilla during recordings in the TG. In the rat tongue, the fungiform papillae are big enough to enable precise stimulation of a single papilla (Yokota and Bradley, 2016). In mice, although the locations of fungiform papillae can be revealed by staining the tongue with food color dyes, it will require precise apparatus to exclusively stimulate a single fungiform papilla without touching the nearby filiform papillae because of the extremely small sizes of the papillae (**Figure S3**). Additionally, single-neuron electrophysiology and tracing could be combined to determine whether the IA-LTMR terminates into a single fungiform papilla. To test the hypothesis that a single TG neuron innervates multiple filiform papillae, sparse labeling of TG neurons could be used together with examination of their nerve terminals in the tongue.

Finally, our study did not explore the behavioral importance of lingual IA- and RA- LTMRs, and we did not compare the functional importance of TG and GG mechanoreceptors innervating the tongue. In the future, it will be important to modulate the activity of LTMRs by optogenetic activation or inhibition acutely, or to ablate LTMR populations using genetic strategies such as diphtheria toxin receptor (DTR) expression, and to see whether the licking, eating and social-grooming behaviors of the animals are affected. It would also be interesting to study whether a change in the filiform papillae patterning will affect animals' ability to sense touch information on the tongue by using transgenic mouse lines with altered filiform papillae patterns (Y. Wang et al., 2016).

Table 1. Genetic screening of Cre driver lines that can label lingual afferents (crossed with *R26*$^{LSL\text{-}tdTom}$)

Genotype	Reported labeling of sensory neuronal subtypes	References	Tamoxifen amount and application time in this study	Expression pattern in the anterior tongue identified in this study
TrkB^{CreERT2}	Aδ LTMRs in DRG and lamellar cells in human Meissner corpuscles	Calavia et al., 2010; Li et al., 2011; Rutlin et al., 2014	0.1 mg @ P0	Flat-shaped cells in the epithelium (could be areas adjacent to fungiform papillae) and cells with dendritic protrusions in the lamina propria

TrkC^{CreERT2}	Proprioceptors and Merkel afferents	Bai et al., 2015; Severson et al., 2017	3 mg @ E12.5; 0.1 mg @ P5 and P6, respectively	Cells in the connective tissue underneath filiform papillae; in E12.5, NFH-negative fibrous structures in deeper muscles were labeled, and some of them were also PGP9.5-negative
Etv1^{CreERT2}	Proprioceptors; Pacinian corpuscle-innervating DRG neurons; Non-myelinating Schwann cells of Pacinian and Meissner corpuscles	de Nooij et al., 2013; Fleming et al., 2016; Prsa et al., 2019	0.1 mg @ P6 - P10	Cells in filiform and fungiform papillae
Vglut1$^{IRES\text{-}cre}$	Proprioceptors and Aβ SA-LTMRs	Brumovsky et al., 2007	N/A	Muscles in the tongue
Advillin^{Cre}	Primary sensory neurons in DRG and TG	Lopes et al., 2017; Zurborg et al., 2011	N/A	Flat-shaped cells in the epithelium of filiform papillae (different from those in *TrkB*^{CreERT2}); Cells with dendritic protrusions in the lamina propria
PV^{Cre}	Proprioceptors; Pacinian, Meissner and lanceolate endings of DRG neurons; TG neurons innervating the tongue	de Nooij et al., 2013; Wu et al., 2018	N/A	Muscles in the tongue (different from *Vglut1*$^{IRES\text{-}cre}$ patterns); Occasionally labels thick fibrous structures that very likely consisted of rod-shaped cells in the lamina propria
TH^{Cre}	C-LTMRs and sympathetic nerves	Li et al., 2011	N/A	Hard to identify individual nerves after 3 days' 6-OHDA treatment
MafA^{Cre}	LTMRs in DRG	Bourane et al., 2009	N/A	Muscles in the tongue
Pirt^{Cre}	Sensory neurons (including GG neurons)	Kim et al., 2008	N/A	Nerve fibers in both fungiform and filiform papillae; Cells within

				and near the taste buds
Vglut2^{Cre}	GG neurons; nociceptors in DRG	Lagerström et al., 2010; Vandenbeuch et al., 2010	N/A	Nerve fibers in both fungiform and filiform papillae

Materials and methods

Animals

All procedures were in accordance with protocols approved by the Johns Hopkins University Animal Care and Use Committee (protocols: MO18M187 and MO21M195). Mice of both genders were used for experiments. For DiI tracing experiments, mice aged from P0 to P22 from both C57BL/6 and CD1 backgrounds were used. For the other experiments, adult mice aged from 6 weeks to 12 months from C57BL/6 background were used, and the mouse lines used in this study included: *Plp1-EGFP* (*B6;CBA-Tg(Plp1-EGFP)10Wmac/J*), *Vglut2*^{Cre} (*B6J.129S6(FVB)-Slc17a6*$^{tm2(cre)Lowl}$*/MwarJ*), *Rosa26*^{Ai9} (*B6.Cg-Gt(ROSA)26Sor*$^{tm9(CAG\text{-}tdTomato)Hze}$*/J*), *Rosa26*^{Ai32} (*B6;129S-Gt(ROSA)26Sor*$^{tm32(CAG\text{-}COP4*H134R/EYFP)Hze}$*/J*), *TrkB*^{CreERT2} (*B6.129S6(Cg)-Ntrk2/J*), *TrkC*^{CreERT2} (*Ntrk3tm3.1(cre/ERT2)Ddg/J*), *Etv1*^{CreERT2} (*B6(Cg)-Etv1tm1.1(cre/ERT2)Zjh/J*), *Vglut1*$^{IRES\text{-}Cre}$ (*B6;129S-Slc17a7tm1.1(cre)Hze/J*), *Advillin*^{Cre} (*B6.129P2-Aviltm2(cre)Fawa/J*), *PV*^{Cre} (*B6;129P2-Pvalbtm1(cre)Arbr/J*), *TH*^{Cre} (*B6.Cg-7630403G23RikTg(Th-cre)1Tmd/J*), *MafA*^{Cre} (Xu et al., n.d.), *Pirt*^{Cre} (Kim et al., 2008), *Vglut2*^{Cre} (*B6J.129S6(FVB)-Slc17a6tm2(cre)Lowl/MwarJ*), *Piezo2-EGFP-IRES-Cre (B6(SJL)-Piezo2tm1.1(cre)Apat/J)* and *Snap25-LSL-2A-EGFP-D (B6.Cg-Snap25tm1.1Hze/J)*. An 8-month-old ferret was used for histological analysis.

To induce CreER-based recombination, tamoxifen was given either in the embryonic stage or to new-born pups. For embryonic stage, A mixture of tamoxifen (3 mg, Toronto Research Chemicals, T006000), progesterone (MilliporeSigma, P0130) and β-estradiol (MilliporeSigma, E8875) in 1:0.5:0.001 ratio prepared in sunflower seed oil (MilliporeSigma, S5007) was administered by oral gavage to pregnant dams. Pups were delivered by Caesarian section at E19-E19.5 and reared by a CD1 foster mother. For new-born pups, 0.1 mg tamoxifen in sunflower seed oil was injected intraperitoneally. The ages of mice when the drug was administered are summarized in **Table 1**.

Histology

Mice were perfused with PBS transcardially followed by 4% PFA. The tissue was further fixed in 4% PFA at 4℃ overnight, and washed in PBS for 3 times afterwards.

For H&E staining, the tissue was dehydrated in 30% sucrose in PBS at 4℃ overnight, and protected by OCT embedding compound before frozen. The tissue was then cryo-sectioned into 8- 10 μm sections on a Leica cryostat. Sections were hydrated in deionized water, stained in Mayer's Hematoxylin Solution (MHS1, Sigma-Aldrich) for 15 min, rinsed in warm running tap water for 15 min, then placed in distilled water for 30 s followed by 95% Reagent Alcohol for 30s. The sections were then placed in Eosin Y Solution (HT110216, Sigma-Aldrich) for 30-60 s. Afterwards, they were dehydrated and cleared through 2 changes of 95% Reagent Alcohol, Reagent Alcohol and xylene for 2 min each. The sections were mounted with Balsam Canada Neutral in Xylene (846578, Carolina Biological Supply Company), and imaged with a Keyence microscope equipped with brightfield illumination.

For Masson-Goldner trichrome staining, the tissue was dehydrated in 30% sucrose in PBS at 4℃ overnight, and protected by OCT embedding compound before frozen. The tissue was then cryosectioned into 8-10 μm sections on a Leica cryostat. Sections were hydrated in deionized water, stained with a Masson-Goldner staining kit (1.00485, Sigma-Aldrich). The sections were mounted with Balsam Canada Neutral in Xylene (846578, Carolina Biological Supply Company), and imaged with a Keyence microscope equipped with brightfield illumination.

For immunostaining tongue, TG and skin sections, the tissue was dehydrated in 30% sucrose in PBS at 4℃ overnight, and protected by OCT embedding compound before frozen. The tissue was then cryo-sectioned into 9-40 um sections on a Leica cryostat. Sections were rehydrated in PBS, permeabilized and blocked by 10% goat serum in 0.3% PBST solution (0.3% Triton X-100 (MilliporeSigma, T9284) in PBS) for 1 hour at room temperature, then incubated with primary antibodies diluted in blocking solution (5% goat serum in 0.3% PBST) at 4℃ overnight. The sections were washed by 0.3% PBST for at least 3 times, 15 min each before incubation with secondary antibodies and DAPI diluted in blocking solution at 4℃ overnight. The tissue was finally washed by 0.3% PBST for at least 3 times and PBS for 1 time, mounted with Poly Aqua-Mount (Polysciences, 18606), and imaged using a confocal microscope (Zeiss LSM 880 or Zeiss LSM 700).

For whole-mount imaging of the dorsal surface of the tongue labeled by a fluorescent dye (1,1'-dioctadecyl-3,3,3',3'-tetramethylindocarbocyanine perchlorate ($DiIC_{18}(3)$), Invitrogen D282) in P1-P10 mice, after fixation, muscles at the ventral side of the tongue were carefully removed by hand with a surgical blade. The tissue was then mounted with Poly Aqua-Mount and imaged with a wide-field microscope (Zeiss Axio Zoom) or a confocal microscope (Zeiss LSM 880). After whole-mount imaging of the dorsal surface, the tissue was cryo-sectioned. The sections were immediately washed with PBS, mounted with Poly Aqua-Mount and imaged using a confocal microscope (Zeiss LSM 880) after sectioning to avoid DiI diffusion.

For whole-mount imaging of the dorsal surface of the tongue labeled by endogenous fluorescent proteins (tdTom) after viral injection in adult mice, after fixation, muscles at the ventral side of the tongue were carefully removed by hand with a surgical blade. The tissue was then cleared by CUBIC Protocol I as described which can preserve endogenous fluorescent proteins during clearing (Tainaka et al., 2018). Briefly, after fixation and washing of the tissue, the tissue was immersed in CUBIC L solution (10% w/v N-butyldiethanolamine (MilliporeSigma, 471240) and

10% w/v Triton X-100 in water) for 3 days at 37℃. It was then washed in PBS overnight at room temperature, followed by immersion in 50% water-diluted CUBIC R solution (45% w/v antipyrine (Tokyo Chemical Industry, D1876) and 30% w/v nicotinamide (Tokyo Chemical Industry, N0078) in water) at room temperature for 1 day. Finally, it was immersed in CUBIC R solution at room temperature for 1-2 days, and imaged with a wide-field microscope (Zeiss Axio Zoom or Olympus BX-41).

For whole-mount imaging of immunostained NFH on the dorsal surface of the tongue, the dorsal surface of tongue was flattened using a method modified from Y. Wang et al. (2016). Freshly dissected tongue was put dorsal side down into a 3-D printed reservoir and was gently pressed against the bottom of the reservoir by a cell strainer (Fisher Scientific, 22-363-549). 4% PFA was added into the reservoir to fix the tissue at 4 ℃ overnight. The flattened tongue was then fixed for another 1 hour at room temperature, washed in PBS for 3 times, embedded in agarose, and its dorsal part was cut into 300 μm sections using a vibratome (HM 650V, Thermo Scientific). The tissue was then stained and cleared using iDISCO method (Renier et al., 2014). Briefly, the tissue was pretreated with a series of methanol/water (20%, 40%, 60%, 80%, 100%) for 1 hour each, then washed further with 100% methanol (MilliporeSigma, 676780) for 1 hour and chilled at 4 ℃. It was then incubated in 66% dichloromethane (MilliporeSigma, 270997)/33% methanol overnight at room temperature with shaking, washed twice in 100% methanol at room temperature on the next day, and chilled at 4 ℃. Then it was bleached in chilled fresh 5% (v/v) hydrogen peroxide (MilliporeSigma, HX0640) in methanol overnight at 4 ℃, rehydrated with methanol/water series on the next day, and washed in PTx.2 (0.2% Triton X-100 in PBS) for 1 hour at room temperature for 2 times. The tissue was then permeabilized by permeabilization solution (23 g/L glycine (MilliporeSigma, G7126) and 20% DMSO (MilliporeSigma, 472301) in PTx.2) at 37 ℃ for 2 days, blocked by blocking solution (6% normal goat serum and 10% DMSO in PTx.2) at 37 ℃ for 2 days, incubated with 1:1000 Chicken anti-NFH in PTwH (0.2% Tween-20, 10 mg/L heparin in PBS)/5%DMSO/3% normal goat serum at 37 ℃ for 7 days, washed in PTwH at 37 ℃ for 4-5 times until the next day, followed by incubation with 1:500 Goat anti-Chicken IgG Alexa Fluor 647 in PTwH/5%DMSO/3% normal goat serum at 37 ℃ for 7 days and washing in PTwH at 37 ℃ for 4-5 times until the next day. Finally, the tissue was dehydrated with methanol/water series for 1 hour each at room temperature, incubated with 66% dichloromethane/33% methanol for 3 hours with shaking at room temperature, and incubated in 100% dichloromethane for 15 minutes twice with shaking to wash away the methanol. The final dehydration steps and the washing steps were done in a petri dish with the tissue sandwiched by two glass slides to preserve the flattened state of the tissue as much as possible. After that, the tissue was immersed in dibenzyl ether (MilliporeSigma, 108014) at room temperature for refraction index matching until it was cleared, and imaged with a confocal microscope (Zeiss LSM 880).

Primary antibodies used in this study and their dilution ratios or concentration are as follows: Chicken anti-NFH 1:1000 (MilliporeSigma AB5539), Rabbit anti-S100 1:50 (Abcam AB76729), Rabbit anti-S100 1:200 (ProteinTech, 15146-1-AP), Rabbit anti-PGP9.5 1:1000 (MilliporeSigma, AB5539), Rabbit anti-NeuN 1:500 (MilliporeSigma, MABN140), Rat anti-Cytokeratin 8 (TROMA-I, DSHB, 2.5 μg/mL).

Secondary antibodies used in this study and their dilution ratios are as follows unless otherwise stated: Goat anti-Rabbit IgG Alexa Fluor 488 1:1000 (ThermoFisher A-11008), Goat anti-Rabbit IgG Alexa Fluor 594 1:1000 (ThermoFisher A-11012), Goat anti-Rabbit IgG Alexa Fluor 647 1:1000 (ThermoFisher A-21244), Goat anti-Chicken IgG Alexa Fluor 488 1:1000 (ThermoFisher A-11309), Goat anti-Chicken IgG Alexa Fluor 647 1:1000 (ThermoFisher A-11039), Goat anti-Rat IgG Alexa Fluor 647 1:1000 (ThermoFisher A-21247).

DiI tracing

For anterograde DiI tracing from TG to tongue, the DiI crystal labeling procedure was modified from Fei et al. (2014). Briefly, after perfusing mice aged P0 - P22 with PBS and 4% PFA, the brain was removed to expose the TG. The dura covering the mandibular branch of TG was pierced through with #5 forceps. $DiIC_{18}(3)$ crystals were implanted into the mandibular region on both left and right sides of the TG, and a few drops of 100% ethanol were added onto the region to dissolve DiI. The head, with the tongue and the TG left *in situ* were covered by a wet paper towel for half an hour, then placed in 4% PFA and incubated at 37℃ for 6 months before the tongue tissue was harvested.

For retrograde DiI tracing from the peripheral to TG for somatotopy, 0.2 μL 0.2 mg/mL DiI solution was injected either into the tip of the tongue or the left whisker pad using a 1 μL micro-syringe (Hamilton). To prepare the DiI solution, $DiIC_{18}(3)$ crystals were dissolved in DMSO to bring 1 mg/mL solution. It was then diluted in PBS by 1:5 to a concentration of 0.2 mg/mL. The animals were sacrificed 5-7 days after DiI injection to enable maximized labeling of neurons.

Surgery

Adult mice (older than 8 weeks) were implanted with titanium head caps ahead of electrophysiological recordings or viral injections in TG. The anesthesia was induced with 3% isoflurane in O_2 and then maintained with 1.5% isoflurane. Mice were kept on a heat blanket (Harvard apparatus), and ophthalmic ointment was applied on eyes to keep them moisturized. 0.5% lidocaine was locally injected under the scalp, and dexamethasone (2 mg/kg) was intraperitoneally injected to prevent inflammation. The skin and the periosteum over the dorsal surface of the skull were removed. A headcap was glued by cyanoacrylic gels (Krazy glue) onto the skull and fixed in place by dental cement. Mice were then injected with buprenorphine (1 mg/kg) i.p. for analgesia and allowed to recover for 7 days. Following headcap implantation, a 2.3 x 2.3 mm cranial window was made with the center located at 2 mm posterior to Bregma, 2 mm lateral to Bregma. The exposed brain region was covered with a biocompatible silicone elastomer (e.g. Kwik-Cast, World Precision Instruments) after craniotomy.

***In vivo* TG electrophysiology**

Mice with head caps were anesthetized by intraperitoneal injection of ketamine/xylazine (87.5 mg/kg and 12.5 mg/kg, respectively), head-fixed, and kept on a heating blanket to maintain its body temperature. The tongue was gently pulled out of the mouth with blunt forceps and put on

a custom-made stable platform with an angle of 30° from the vertical. The accessible length of the tongue on the platform was 2.5 - 3 mm. The images of the tongue stained by food color dyes were captured with a circuit board USB digital microscope (Chipquick, SMDPMUSB413). To keep the surface of the tongue moisturized, artificial saliva (4 mM NaCl, 10 mM KCl, 6 mM $KHCO_3$, 6 mM $NaHCO_3$, 0.5 mM $CaCl_2$, 0.5 mM $MgCl_2$, 0.24 mM K_2HPO_4, 0.24 mM KH_2PO_4, pH 7.5. Zocchi et al., 2017) at room temperature was applied on the tongue every now and then. A 2 MΩ tungsten electrode (World Precision Instruments, TM33A20) driven by a Sutter manipulator was inserted into the depth of TG (around 5 - 6 mm below brain surface). A reference 2 MΩ electrode was placed outside the craniotomy covered in sterile saline. The differential signal between the recording and the reference electrodes was amplified 10,000x, band-pass filtered between 300 Hz to 3,000 Hz, and acquired at 20 kHz. In order to find tongue units, multiple TG locations surrounding 2.3 mm posterior to Bregma, 2 mm lateral to Bregma were probed. While the electrode was moving down at the depth of TG, the orofacial regions of the mouse including whisker pad, cheek, lower jaw and tongue were touched by a hand-held fine-tip brush in a stroking manner in order to reveal the receptive fields of the units encountered. Once a unit that could respond only to tactile stimuli on the tongue was discovered, it was further tested with von Frey filaments, chemicals, and ice-cold artificial saliva. To test the conduction velocity of the unit, a 0.4 mA, 1 ms electric pulse generated by a stimulus isolator (World Precision Instruments, A365) was delivered onto the unit's receptive field by a concentric bipolar electrode (World Precision Instruments, TM33CCINS). For opto-tagging experiments, 10 ms-long light pulses were generated by a 473 nm DPSS laser (Laserglow Technologies, R471003GX) and delivered to the tongue via a 200 mm, 0.39 NA optical fiber manually positioned around 1 mm away from the unit's receptive field, with the actual power to be 15 -18 mW. The TTL inputs sent to the stimulus isolator and the laser were generated from a National Instruments DAQ system (BNC-2090A), and were recorded by Wavesurfer (https://wavesurfer.janelia.org/) together with electrophysiological data. When a unit was found with a RF located near the edge of the tongue, it was further probed with tactile and optical stimulus at both ventral and dorsal sides of the tongue to determine its exact RF location. The mice were redosed with 25-50% of the initial ketamine/xylazine once they started to wake up from anesthesia indicated by whisker twitching. The duration of anesthetic state of the mouse between each redose was closely monitored in order to avoid applying excessive doses.

Chemicals applied on the tongue surface include: tannic acid (100, 200, 500, 1000 μM, diluted with artificial saliva, MilliporeSigma, 403040), (−)-epigallocatechin gallate (EGCG, 100, 200, 500, 1000 μM, diluted with artificial saliva, MilliporeSigma, E4143), Hydroxy-α-sanshool (1900 μM, freshly dissolved in DMSO and then diluted with artificial saliva by 1:20. Medchemexpress, HY-N6825), Kava concentrate (commercial drink, Kalm with Kava™, iced tea flavor).

Data processing Voltage recordings were high-pass filtered at 300 Hz with custom designed filters using MATLAB R2018a (MathWorks), thresholded, and clustered using MClust 4.4 (made by A. D. Redish, https://github.com/adredish/MClust-Spike-Sorting-Toolbox) to extract single unit waveforms. Units whose RFs were located at the ventral side of the tongue were disregarded for analysis.

Viral injection in the TG

Glass pipettes (Wiretrol II, Drummond Scientific Company, 5-000-2010) with a long taper (more than 6 mm) were pulled with a pipette puller (Sutter Instruments, model P-97) for TG injection, their tips trimmed by forceps and then beveled by gently being pressed against a rotating disk. A hydraulic microinjection system was used for injection. For labeling a fair number (tens to hundreds) of mandibular branch neurons, the pipette containing AAVPHP.S-CAG-FLEX-tdTomato virus (Addgene 28306-PHP.S, $1.8x10^{13}$ vg/mL) targeted at 2 locations in the mandibular branch spaced 250 um apart. For each injection site, 200 nL virus was injected at a rate of 70 nL/min at 5.4 mm and 5.8 mm depths, respectively. The craniotomy was then covered and protected by silicon elastomers and the mice were sacrificed 3 weeks after viral injection.

Piezo2 expression of tongue-innervating neurons

The tongue tissue was collected from *Piezo2-EGFP-IRES-Cre/+;Snap25*$^{LSL\text{-}EGFP/+}$ mice at P1-P2 after decapitation and was freshly embedded in low-melt agarose (2% at 40℃) with the dorsal side facing up, followed by imaging with a confocal microscope. To avoid linage problems caused by embryonic expression of Piezo2, other mice that were *Piezo2-EGFP-IRES-Cre/+;Snap25*$^{LSL\text{-}EGFP/+}$ or *Piezo2-EGFP-IRES-Cre/+;Snap25*$^{+/+}$ were injected with AAV9-pCAG-FLEX-tdTomato-WPRE interperitoneally (10μl, 6.4x1012 GC/ml). The tissue was harvested 14 days after injections. The green autofluorescence and the tdTomato expression at the dorsal surface of the tongue were imaged with a confocal microscope. The autofluorescence signals from the filiform papillae were subtracted from the red channel with Fiji.

AAV9-pCAG-FLEX-tdTomato-WPRE was a gift from Hongkui Zeng (Addgene plasmid # 51503) and was produced by Vigene Biosciences.

Statistical analysis and data processing

All analyses were performed using Python unless stated otherwise. No statistical methods were used to predetermine sample sizes. Results were presented as mean ± S.D. unless stated otherwise. The confocal and wide-field fluorescence images were processed using ImageJ.

Acknowledgements

We thank Xinzhong Dong for providing *Pirt*^{Cre} and *MafA*^{Cre} mice, Wenqin Luo for providing *Split*^{Cre} mice, Kristina Nielsen and Jennifer Smith for providing fixed ferret tongue tissue. We thank Varun Chokshi and Jeong Jun Kim for comments on the manuscript. This work was supported by NIH grants R01NS089652 and 1R01NS104834-01 (D.H.O.) and by the intramural program of the NIH, the National Center for Complementary and Integrative Health, and National Institute of Neurological Disorders and Stroke (A.T.C.).

Author contributions

L.Z., W.P.O. and D.H.O. planned the project and designed experiments. L.Z. collected and analyzed data under the supervision of D.H.O. M.N. collected the data showing Piezo2 expression in the tongue under the supervision of A.T.C. L.Z. wrote the initial draft of the paper with inputs from all authors. All authors discussed and edited the paper.

Declaration of interests

The authors declare no competing interests.

References

Abraira, V.E., Ginty, D.D., 2013. The sensory neurons of touch. Neuron 79, 618–639. https://doi.org/10.1016/j.neuron.2013.07.051

Aktar, T., Chen, J., Ettelaie, R., Holmes, M., 2015. Tactile Sensitivity and Capability of Soft-Solid Texture Discrimination. J. Texture Stud. 46, 429–439. https://doi.org/10.1111/jtxs.12142

Bai, L., Lehnert, B.P., Liu, J., Neubarth, N.L., Dickendesher, T.L., Nwe, P.H., Cassidy, C., Woodbury, C.J., Ginty, D.D., 2015. Genetic identification of an expansive mechanoreceptor sensitive to skin stroking. Cell 163, 1783–1795. https://doi.org/10.1016/j.cell.2015.11.060

Bangcuyo, R.G., Simons, C.T., 2017. Lingual tactile sensitivity: effect of age group, sex, and fungiform papillae density. Exp. Brain Res. 235, 2679–2688. https://doi.org/10.1007/s00221-017-5003-7

Bautista, D.M., Siemens, J., Glazer, J.M., Tsuruda, P.R., Basbaum, A.I., Stucky, C.L., Jordt, S.-E., Julius, D., 2007. The menthol receptor TRPM8 is the principal detector of environmental cold. Nature 448, 204–208. https://doi.org/10.1038/nature05910

Blom, S., 1960. Afferent influences on tongue muscle activity. A morphological and physiological study in the cat. Acta Physiol. Scand. Suppl. 49, 1–97.

Böck, P., 1971. Nerves of the papilla filiformis of the tongue of the guinea pig. Arch. Histol. Jpn. Nihon Soshikigaku Kiroku 32, 399–411.

Bourane, S., Garces, A., Venteo, S., Pattyn, A., Hubert, T., Fichard, A., Puech, S., Boukhaddaoui, H., Baudet, C., Takahashi, S., Valmier, J., Carroll, P., 2009. Low-Threshold Mechanoreceptor Subtypes Selectively Express MafA and Are Specified by Ret Signaling. Neuron 64, 857–870. https://doi.org/10.1016/j.neuron.2009.12.004

Brumovsky, P., Watanabe, M., Hökfelt, T., 2007. Expression of the vesicular glutamate transporters-1 and -2 in adult mouse dorsal root ganglia and spinal cord and their regulation by nerve injury. Neuroscience 147, 469–490. https://doi.org/10.1016/j.neuroscience.2007.02.068

Calavia, M.G., Feito, J., López-Iglesias, L., de Carlos, F., García-Suarez, O., Pérez-Piñera, P., Cobo, J., Vega, J.A., 2010. The lamellar cells in human Meissner corpuscles express TrkB. Neurosci. Lett. 468, 106–109. https://doi.org/10.1016/j.neulet.2009.10.076

Chee, C., Arshad, S., Singh, S., Mistry, S., Hamdy, S., 2005. The influence of chemical gustatory stimuli and oral anaesthesia on healthy human pharyngeal swallowing. Chem. Senses 30, 393–400. https://doi.org/10.1093/chemse/bji034

Chesler, A.T., Szczot, M., Bharucha-Goebel, D., Čeko, M., Donkervoort, S., Laubacher, C., Hayes, L.H., Alter, K., Zampieri, C., Stanley, C., Innes, A.M., Mah, J.K., Grosmann, C.M., Bradley, N., Nguyen, D., Foley, A.R., Le Pichon, C.E., Bönnemann, C.G., 2016. The Role of PIEZO2 in Human Mechanosensation. N. Engl. J. Med. 375, 1355–1364. https://doi.org/10.1056/NEJMoa1602812

de Nooij, J.C., Doobar, S., Jessell, T.M., 2013. Etv1 Inactivation Reveals Proprioceptor Subclasses that Reflect the Level of NT3 Expression in Muscle Targets. Neuron 77,

1055–1068. https://doi.org/10.1016/j.neuron.2013.01.015
Donnelly, C.R., Kumari, A., Li, L., Vesela, I., Bradley, R.M., Mistretta, C.M., Pierchala, B.A., 2022. Probing the multimodal fungiform papilla: complex peripheral nerve endings of chorda tympani taste and mechanosensitive fibers before and after Hedgehog pathway inhibition. Cell Tissue Res. 387, 225–247. https://doi.org/10.1007/s00441-021-03561-1
Donnelly, C.R., Shah, A.A., Mistretta, C.M., Bradley, R.M., Pierchala, B.A., 2018. Biphasic functions for the GDNF-Ret signaling pathway in chemosensory neuron development and diversification. Proc. Natl. Acad. Sci. 115, E516–E525. https://doi.org/10.1073/pnas.1708838115
Engelen, L., de Wijk, R.A., Prinz, J.F., Janssen, A.M., Weenen, H., Bosman, F., 2003. The effect of oral and product temperature on the perception of flavor and texture attributes of semi-solids. Appetite 41, 273–281. https://doi.org/10.1016/S0195-6663(03)00105-3
Essick, G.K., Chopra, A., Guest, S., McGlone, F., 2003. Lingual tactile acuity, taste perception, and the density and diameter of fungiform papillae in female subjects. Physiol. Behav. 80, 289–302. https://doi.org/10.1016/j.physbeh.2003.08.007
Fei, D., Huang, T., Krimm, R.F., 2014. The neurotrophin receptor p75 regulates gustatory axon branching and promotes innervation of the tongue during development. Neural Develop. 9, 15. https://doi.org/10.1186/1749-8104-9-15
Fleming, M.S., Li, J.J., Ramos, D., Li, T., Talmage, D.A., Abe, S., Arber, S., Luo, W., 2016. A RET-ER81-NRG1 Signaling Pathway Drives the Development of Pacinian Corpuscles. J. Neurosci. 36, 10337–10355. https://doi.org/10.1523/JNEUROSCI.2160-16.2016
Godement, P., Vanselow, J., Thanos, S., Bonhoeffer, F., 1987. A study in developing visual systems with a new method of staining neurones and their processes in fixed tissue. Dev. Camb. Engl. 101, 697–713. https://doi.org/10.1242/dev.101.4.697
Goździewska-Harłajczuk, K., Klećkowska-Nawrot, J., Barszcz, K., Marycz, K., Nawara, T., Modlińska, K., Stryjek, R., 2018. Biological aspects of the tongue morphology of wild-captive WWCPS rats: a histological, histochemical and ultrastructural study. Anat. Sci. Int. 93, 514–532. https://doi.org/10.1007/s12565-018-0445-y
Honig, M.G., Hume, R.I., 1986. Fluorescent carbocyanine dyes allow living neurons of identified origin to be studied in long-term cultures. J. Cell Biol. 103, 171–187. https://doi.org/10.1083/jcb.103.1.171
Iwasaki, S., Okumura, Y., Kumakura, M., 1999. Ultrastructural Study of the Relationship between the Morphogenesis of Filiform Papillae and the Keratinization of the Lingual Epithelium in the Mouse. Cells Tissues Organs 165, 91–103. https://doi.org/10.1159/000016679
Kim, A.Y., Tang, Z., Liu, Q., Patel, K.N., Maag, D., Geng, Y., Dong, X., 2008. Pirt, a phosphoinositide-binding protein, functions as a regulatory subunit of TRPV1. Cell 133, 475–485. https://doi.org/10.1016/j.cell.2008.02.053
Kim, Y.S., Anderson, M., Park, K., Zheng, Q., Agarwal, A., Gong, C., Saijilafu, Young, L., He, S., LaVinka, P.C., Zhou, F., Bergles, D., Hanani, M., Guan, Y., Spray, D.C., Dong, X., 2016. Coupled Activation of Primary Sensory Neurons Contributes to Chronic Pain. Neuron 91, 1085–1096. https://doi.org/10.1016/j.neuron.2016.07.044
Kim, Y.S., Kim, T.H., McKemy, D.D., Bae, Y.C., 2015. Expression of vesicular glutamate transporters in transient receptor potential melastatin 8 (TRPM8)-positive dental afferents in the mouse. Neuroscience 303, 378–388. https://doi.org/10.1016/j.neuroscience.2015.07.013
Kunze, K., 1969. The filiform papilla in man as a tactile sense organ. Light and electron microscopic studies. Ergeb. Anat. Entwicklungsgesch. 41, 3–64.
Kuroki, S., Hagura, N., Nishida, S., Haggard, P., Watanabe, J., 2016. Sanshool on The Fingertip Interferes with Vibration Detection in a Rapidly-Adapting (RA) Tactile Channel. PLOS ONE 11, e0165842. https://doi.org/10.1371/journal.pone.0165842

Lagerström, M.C., Rogoz, K., Abrahamsen, B., Persson, E., Reinius, B., Nordenankar, K., Olund, C., Smith, C., Mendez, J.A., Chen, Z.-F., Wood, J.N., Wallén-Mackenzie, A., Kullander, K., 2010. VGLUT2-dependent sensory neurons in the TRPV1 population regulate pain and itch. Neuron 68, 529–542. https://doi.org/10.1016/j.neuron.2010.09.016

Lauga, E., Pipe, C.J., Le Révérend, B., 2016. Sensing in the Mouth: A Model for Filiform Papillae as Strain Amplifiers. Front. Phys. 4. https://doi.org/10.3389/fphy.2016.00035

Leijon, S.C.M., Neves, A.F., Breza, J.M., Simon, S.A., Chaudhari, N., Roper, S.D., 2019. Oral thermosensing by murine trigeminal neurons: modulation by capsaicin, menthol and mustard oil. J. Physiol. 597, 2045–2061. https://doi.org/10.1113/JP277385

Li, L., Rutlin, M., Abraira, V.E., Cassidy, C., Kus, L., Gong, S., Jankowski, M.P., Luo, W., Heintz, N., Koerber, H.R., Woodbury, C.J., Ginty, D.D., 2011. The functional organization of cutaneous low-threshold mechanosensory neurons. Cell 147, 1615–1627. https://doi.org/10.1016/j.cell.2011.11.027

Lopes, D.M., Denk, F., McMahon, S.B., 2017. The Molecular Fingerprint of Dorsal Root and Trigeminal Ganglion Neurons. Front. Mol. Neurosci. 10. https://doi.org/10.3389/fnmol.2017.00304

Luo, J., Ke, J., Hou, X., Li, S., Luo, Q., Wu, H., Shen, G., Zhang, Z., 2022. Composition, structure and flavor mechanism of numbing substances in Chinese prickly ash in the genus Zanthoxylum: A review. Food Chem. 373, 131454. https://doi.org/10.1016/j.foodchem.2021.131454

Miles, B.L., Van Simaeys, K., Whitecotton, M., Simons, C.T., 2018. Comparative tactile sensitivity of the fingertip and apical tongue using complex and pure tactile tasks. Physiol. Behav. 194, 515–521. https://doi.org/10.1016/j.physbeh.2018.07.002

Moayedi, Y., Duenas-Bianchi, L.F., Lumpkin, E.A., 2018. Somatosensory innervation of the oral mucosa of adult and aging mice. Sci. Rep. 8, 1–14. https://doi.org/10.1038/s41598-018-28195-2

Moayedi, Y., Xu, S., Obayashi, S.K., Hoffman, B.U., Gerling, G.J., Lumpkin, E.A., 2023. The cellular basis of mechanosensation in mammalian tongue. Cell Rep. 42. https://doi.org/10.1016/j.celrep.2023.112087

Mountcastle, V.B., Talbot, W.H., Darian-Smith, I., Kornhuber, H.H., 1967. Neural Basis of the Sense of Flutter-Vibration. Science 155, 597–600.

Nguyen, M.Q., Wu, Y., Bonilla, L.S., Buchholtz, L.J. von, Ryba, N.J.P., 2017. Diversity amongst trigeminal neurons revealed by high throughput single cell sequencing. PLOS ONE 12, e0185543. https://doi.org/10.1371/journal.pone.0185543

Niemi, M., Laaksonen, J.-P., Vähätalo, K., Tuomainen, J., Aaltonen, O., Happonen, R.-P., 2002. Effects of transitory lingual nerve impairment on speech: an acoustic study of vowel sounds. J. Oral Maxillofac. Surg. Off. J. Am. Assoc. Oral Maxillofac. Surg. 60, 647–652; discussion 653. https://doi.org/10.1053/joms.2002.33113

Ohman-Gault, L., Huang, T., Krimm, R., 2017. The transcription factor Phox2b distinguishes between oral and non-oral sensory neurons in the geniculate ganglion. J. Comp. Neurol. 525, 3935–3950. https://doi.org/10.1002/cne.24312

Okubo, T., Clark, C., Hogan, B.L.M., 2009. Cell Lineage Mapping of Taste Bud Cells and Keratinocytes in the Mouse Tongue and Soft Palate. Stem Cells Dayt. Ohio 27, 442–450. https://doi.org/10.1634/stemcells.2008-0611

Patel, K.N., Liu, Q., Meeker, S., Undem, B.J., Dong, X., 2011. Pirt, a TRPV1 modulator, is required for histamine-dependent and -independent itch. PloS One 6, e20559. https://doi.org/10.1371/journal.pone.0020559

Pippi, R., Spota, A., Santoro, M., 2018. Medicolegal Considerations Involving Iatrogenic Lingual Nerve Damage. J. Oral Maxillofac. Surg. 76, 1651.e1-1651.e13. https://doi.org/10.1016/j.joms.2018.03.020

Prsa, M., Morandell, K., Cuenu, G., Huber, D., 2019. Feature-selective encoding of substrate vibrations in the forelimb somatosensory cortex. Nature 567, 384. https://doi.org/10.1038/s41586-019-1015-8

Ranade, S.S., Woo, S.-H., Dubin, A.E., Moshourab, R.A., Wetzel, C., Petrus, M., Mathur, J., Bégay, V., Coste, B., Mainquist, J., Wilson, A.J., Francisco, A.G., Reddy, K., Qiu, Z., Wood, J.N., Lewin, G.R., Patapoutian, A., 2014. Piezo2 is the major transducer of mechanical forces for touch sensation in mice. Nature 516, 121–125. https://doi.org/10.1038/nature13980

Reginato, G. de S., Bolina, C. de S., Watanabe, I., Ciena, A.P., 2014. Three-Dimensional Aspects of the Lingual Papillae and Their Connective Tissue Cores in the Tongue of Rats: A Scanning Electron Microscope Study. Sci. World J. 2014, 841879. https://doi.org/10.1155/2014/841879

Renier, N., Wu, Z., Simon, D.J., Yang, J., Ariel, P., Tessier-Lavigne, M., 2014. iDISCO: A Simple, Rapid Method to Immunolabel Large Tissue Samples for Volume Imaging. Cell 159, 896–910. https://doi.org/10.1016/j.cell.2014.10.010

Rutlin, M., Ho, C.-Y., Abraira, V.E., Cassidy, C., Bai, L., Woodbury, C.J., Ginty, D.D., 2014. The Cellular and Molecular Basis of Direction Selectivity of Aδ-LTMRs. Cell 159, 1640–1651. https://doi.org/10.1016/j.cell.2014.11.038

Sato, O., Maeda, T., Kobayashi, S., Iwanaga, T., Fujita, T., 1988. Filiform papillae as a sensory apparatus in the tongue: An immunohistochemical study of nervous elements by use of neurofilamcnt protein (NFP) and S-100 protein antibodies. Cell Tissue Res. 252, 231–238. https://doi.org/10.1007/BF00214365

Schöbel, N., Radtke, D., Kyereme, J., Wollmann, N., Cichy, A., Obst, K., Kallweit, K., Kletke, O., Minovi, A., Dazert, S., Wetzel, C.H., Vogt-Eisele, A., Gisselmann, G., Ley, J.P., Bartoshuk, L.M., Spehr, J., Hofmann, T., Hatt, H., 2014. Astringency is a trigeminal sensation that involves the activation of G protein-coupled signaling by phenolic compounds. Chem. Senses 39, 471–487. https://doi.org/10.1093/chemse/bju014

Severson, K.S., Xu, D., Van de Loo, M., Bai, L., Ginty, D.D., O'Connor, D.H., 2017. Active touch and self-motion encoding by Merkel cell-associated afferents. Neuron 94, 666-676.e9. https://doi.org/10.1016/j.neuron.2017.03.045

Spassova, I., 1974. Ultrastructure of the simple encapsulated nerve endings (simple end-bulbs of Krause) in the tongue of the cat. J. Anat. 118, 1–9.

Stern, J.M., Johnson, S.K., 1989. Perioral somatosensory determinants of nursing behavior in Norway rats (Rattus norvegicus). J. Comp. Psychol. 103, 269–280. https://doi.org/10.1037/0735-7036.103.3.269

Suemune, S., Nishimori, T., Hosoi, M., Suzuki, Y., Tsuru, H., Kawata, T., Yamauchi, K., Maeda, N., 1992. Trigeminal nerve endings of lingual mucosa and musculature of the rat. Brain Res. 586, 162–165. https://doi.org/10.1016/0006-8993(92)91389-V

Tainaka, K., Murakami, T.C., Susaki, E.A., Shimizu, C., Saito, R., Takahashi, K., Hayashi-Takagi, A., Sekiya, H., Arima, Y., Nojima, S., Ikemura, M., Ushiku, T., Shimizu, Y., Murakami, M., Tanaka, K.F., Iino, M., Kasai, H., Sasaoka, T., Kobayashi, K., Miyazono, K., Morii, E., Isa, T., Fukayama, M., Kakita, A., Ueda, H.R., 2018. Chemical Landscape for Tissue Clearing Based on Hydrophilic Reagents. Cell Rep. 24, 2196-2210.e9. https://doi.org/10.1016/j.celrep.2018.07.056

Tei, K., Yamazaki, Y., Kobayashi, M., Izumiyama, Y., Ono, M., Totsuka, Y., 2004. Effects of bilateral lingual and inferior alveolar nerve anesthesia effects on masticatory function and early swallowing. Oral Surg. Oral Med. Oral Pathol. Oral Radiol. Endod. 97, 553–558. https://doi.org/10.1016/S1079210403006875

Trulsson, M., Essick, G.K., 2010. Sensations Evoked by Microstimulation of Single Mechanoreceptive Afferents Innervating the Human Face and Mouth. J. Neurophysiol. 103, 1741–1747. https://doi.org/10.1152/jn.01146.2009

Trulsson, M., Essick, G.K., 1997. Low-threshold mechanoreceptive afferents in the human lingual nerve. J. Neurophysiol. 77, 737–748. https://doi.org/10.1152/jn.1997.77.2.737
Vandenbeuch, A., Tizzano, M., Anderson, C.B., Stone, L.M., Goldberg, D., Kinnamon, S.C., 2010. Evidence for a role of glutamate as an efferent transmitter in taste buds. BMC Neurosci. 11, 77. https://doi.org/10.1186/1471-2202-11-77
von Buchholtz, L.J. von, Ghitani, N., Lam, R.M., Licholai, J.A., Chesler, A.T., Ryba, N.J.P., 2021. Decoding Cellular Mechanisms for Mechanosensory Discrimination. Neuron 109, 285-298.e5. https://doi.org/10.1016/j.neuron.2020.10.028
Wang, B., Yang, W., McKittrick, J., Meyers, M.A., 2016. Keratin: Structure, mechanical properties, occurrence in biological organisms, and efforts at bioinspiration. Prog. Mater. Sci. 76, 229–318. https://doi.org/10.1016/j.pmatsci.2015.06.001
Wang, Y., 1993. Selectivity of lingual nerve fibers to chemical stimuli. J. Gen. Physiol. 101, 843–866. https://doi.org/10.1085/jgp.101.6.843
Wang, Y., Erickson, R.P., Simon, S.A., 1993. Selectivity of lingual nerve fibers to chemical stimuli. J. Gen. Physiol. 101, 843–866. https://doi.org/10.1085/jgp.101.6.843
Wang, Y., Williams, J., Rattner, A., Wu, S., Bassuk, A.G., Goffinet, A.M., Nathans, J., 2016. Patterning of papillae on the mouse tongue: A system for the quantitative assessment of planar cell polarity signaling. Dev. Biol. 419, 298–310. https://doi.org/10.1016/j.ydbio.2016.09.004
Whitehead, M.C., Beeman, C.S., Kinsella, B.A., 1985. Distribution of taste and general sensory nerve endings in fungiform papillae of the hamster. Am. J. Anat. 173, 185–201. https://doi.org/10.1002/aja.1001730304
Wilkinson, G.A., Fariñas, I., Backus, C., Yoshida, C.K., Reichardt, L.F., 1996. Neurotrophin-3 Is a Survival Factor In Vivo for Early Mouse Trigeminal Neurons. J. Neurosci. 16, 7661–7669. https://doi.org/10.1523/JNEUROSCI.16-23-07661.1996
Wu, A., Dvoryanchikov, G., Pereira, E., Chaudhari, N., Roper, S.D., 2015. Breadth of tuning in taste afferent neurons varies with stimulus strength. Nat. Commun. 6, 8171. https://doi.org/10.1038/ncomms9171
Wu, P., Arris, D., Grayson, M., Hung, C.-N., Ruparel, S., 2018. Characterization of sensory neuronal subtypes innervating mouse tongue. PLOS ONE 13, e0207069. https://doi.org/10.1371/journal.pone.0207069
Xu, Q., Ford, N.C., He, S., Huang, Q., Anderson, M., Chen, Z., Yang, F., Crawford, L.K., Caterina, M.J., Guan, Y., Dong, X., n.d. Astrocytes contribute to pain gating in the spinal cord. Sci. Adv. 7, eabi6287. https://doi.org/10.1126/sciadv.abi6287
Yackinous, C., Guinard, J.-X., 2001. Relation between PROP taster status and fat perception, touch, and olfaction. Physiol. Behav. 72, 427–437. https://doi.org/10.1016/S0031-9384(00)00430-3
Yokota, Y., Bradley, R.M., 2016. Receptive field size, chemical and thermal responses, and fiber conduction velocity of rat chorda tympani geniculate ganglion neurons. J. Neurophysiol. 115, 3062–3072. https://doi.org/10.1152/jn.00045.2016
Zhang, G.-H., Zhang, H.-Y., Deng, S.-P., Qin, Y.-M., 2008. Regional Differences in Taste Bud Distribution and α-Gustducin Expression Patterns in the Mouse Fungiform Papilla. Chem. Senses 33, 357–362. https://doi.org/10.1093/chemse/bjm093
Zhou, X., Yeomans, M., Thomas, A., Wilde, P., Linter, B., Methven, L., 2021. Individual differences in oral tactile sensitivity and gustatory fatty acid sensitivity and their relationship with fungiform papillae density, mouth behaviour and texture perception of a food model varying in fat. Food Qual. Prefer. 90, 104116. https://doi.org/10.1016/j.foodqual.2020.104116
Zocchi, D., Wennemuth, G., Oka, Y., 2017. The cellular mechanism for water detection in the mammalian taste system. Nat. Neurosci. 20, 927–933. https://doi.org/10.1038/nn.4575
Zurborg, S., Piszczek, A., Martínez, C., Hublitz, P., Al Banchaabouchi, M., Moreira, P., Perlas,

E., Heppenstall, P.A., 2011. Generation and characterization of an Advillin-Cre driver mouse line. Mol. Pain 7, 66. https://doi.org/10.1186/1744-8069-7-66

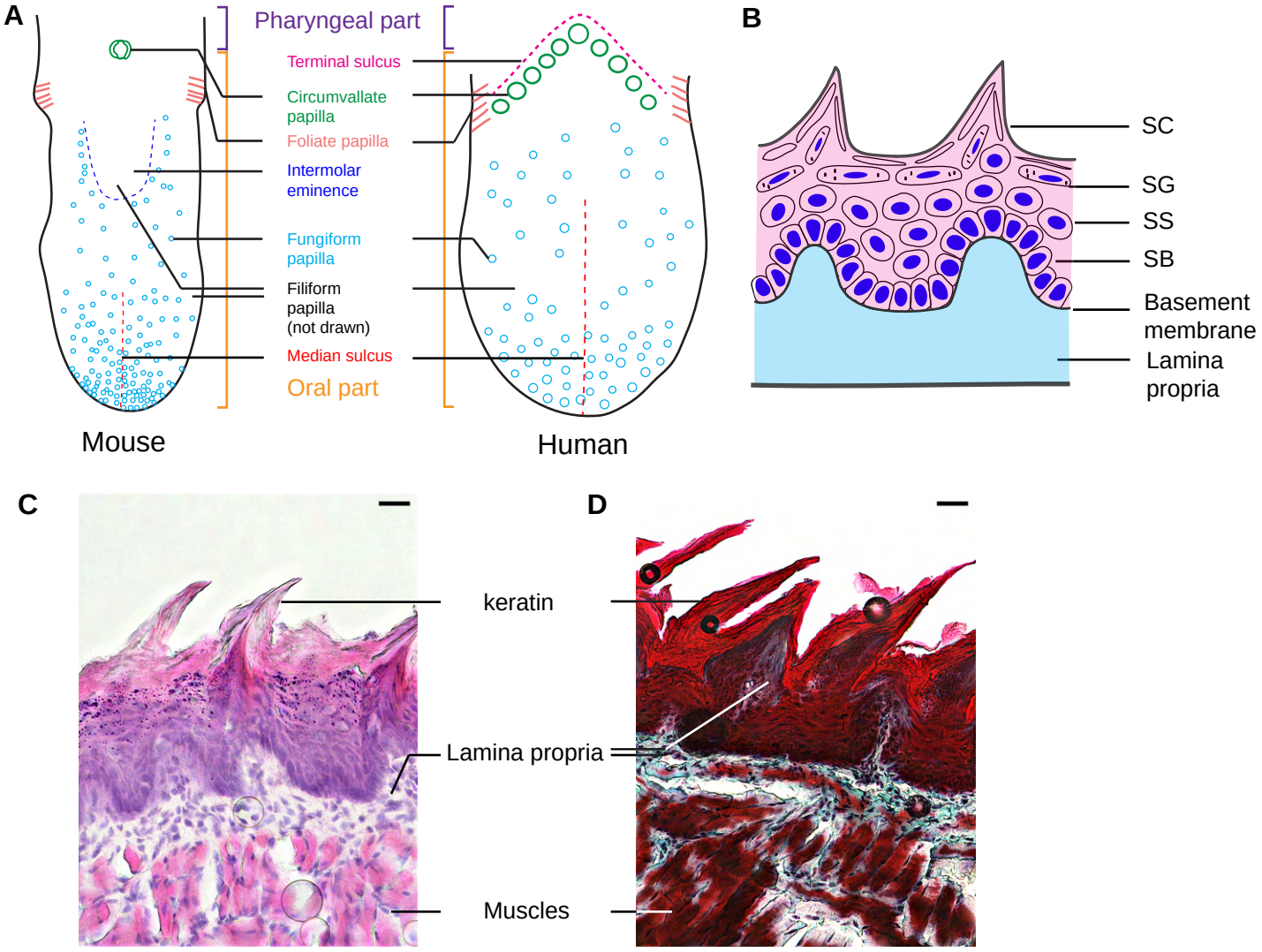

Figure 1. The anatomy of the tongue
(A) Left: a schematic outlined from an actual mouse tongue with DiI anterograde tracing from the TG to reveal locations of lingual papillae. Filiform papillae are the most abundant type among the four types of papillae and are distributed across the entire oral part of the tongue, including the intermolar eminence. They are not seen at the pharyngeal part of the tongue posterior to the circumvallate papilla. Fungiform papillae are distributed across the anterior part of the tongue and regions surrounding the intermolar eminence, but not inside or posterior to the intermolar eminence.
Right: a schematic of the human tongue modified from Jung et al. (2004). The exact numbers and locations of the lingual papillae (especially the fungiform papillae) may not match those of the real tongue.
The sizes of the tongues are out of scale.
(B) A schematic diagram of the keratinized oral mucosa. SC: stratum corneum. SG: stratum granulosum. SS: stratum spinosum. SB: stratum basale. Blue: cell nuclei. Pink: epithelium. Cyan: lamina propria.
(C) Lingual mucosa of a 6-week-old mouse stained with H&E. Cell nuclei were stained purple, and proteins were stained pink. Keratin composed of dead epithelial cells was almost transparent. Scale bar: 25 µm.
(D) Lingual mucosa of a 6-week-old mouse stained with Masson-Goldner staining. Keratin was stained bright red. The lamina propria (connective tissue) stained cyan infiltrated each filiform papilla until reaching the keratin layer. The muscles were stained dark red. Scale bar: 25 µm.

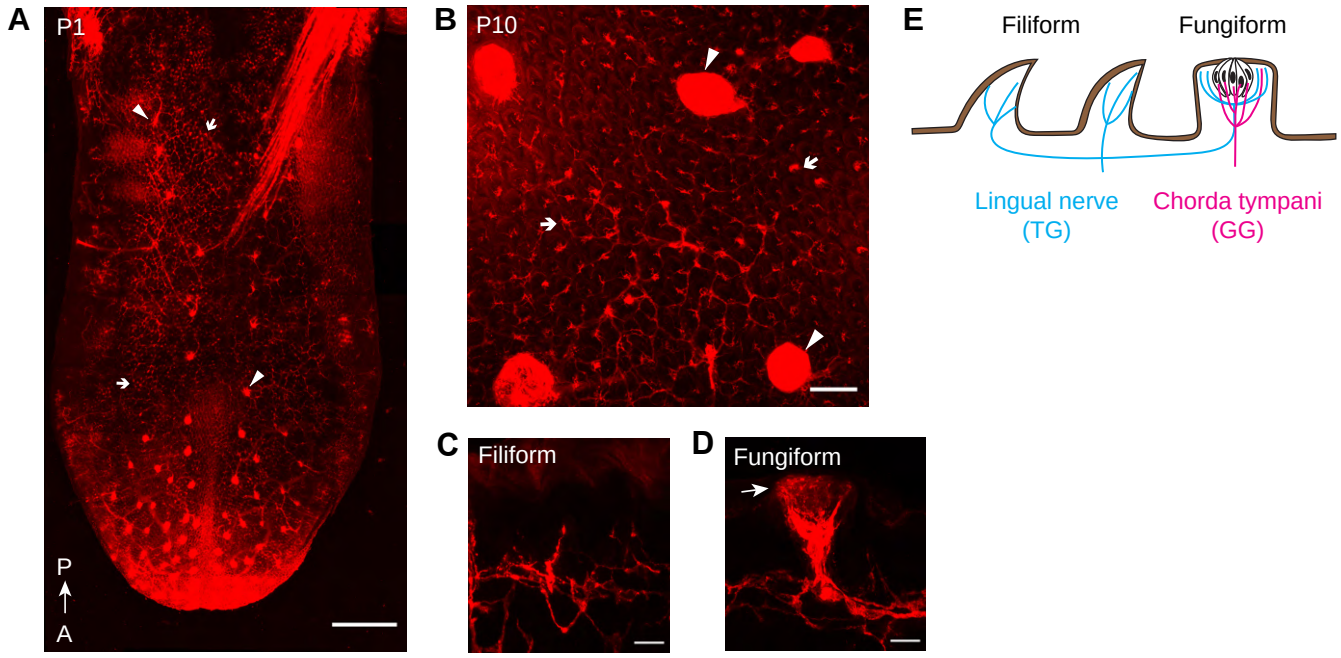

Figure 2. Trigeminal ganglion projects to both filiform papillae and fungiform papillae in the mouse tongue
(A-B) Dorsal views of the tongue showing DiI-labeled trigeminal axons in P1 **(A)** and P10 **(B)** mice. Arrows: filiform papillae. Triangles: fungiform papillae. To reveal the fluorescent signals in the filiform papillae in **(B)**, those in the fungiform papillae were saturated due to contrast adjustments. Scale bar: 500 µm for **(A)** and 100 µm for **(B)**.
(C-D) Cross-section views of the tongue showing DiI-labeled trigeminal axons in filiform **(C)** and fungiform **(D)** papillae. The arrow in **(D)**: axons terminated at the extragemmal regions of a fungiform papilla. Scale bar: 20 µm.
(E) A schematic of the innervation patterns of trigeminal ganglion (TG) neurons and geniculate ganglion (GG) neurons on filiform and fungiform papillae. Fungiform papillae are innervated by both chorda tympani nerve from GG and lingual nerve from TG, whereas filiform papillae are only innervated by lingual nerve from TG.

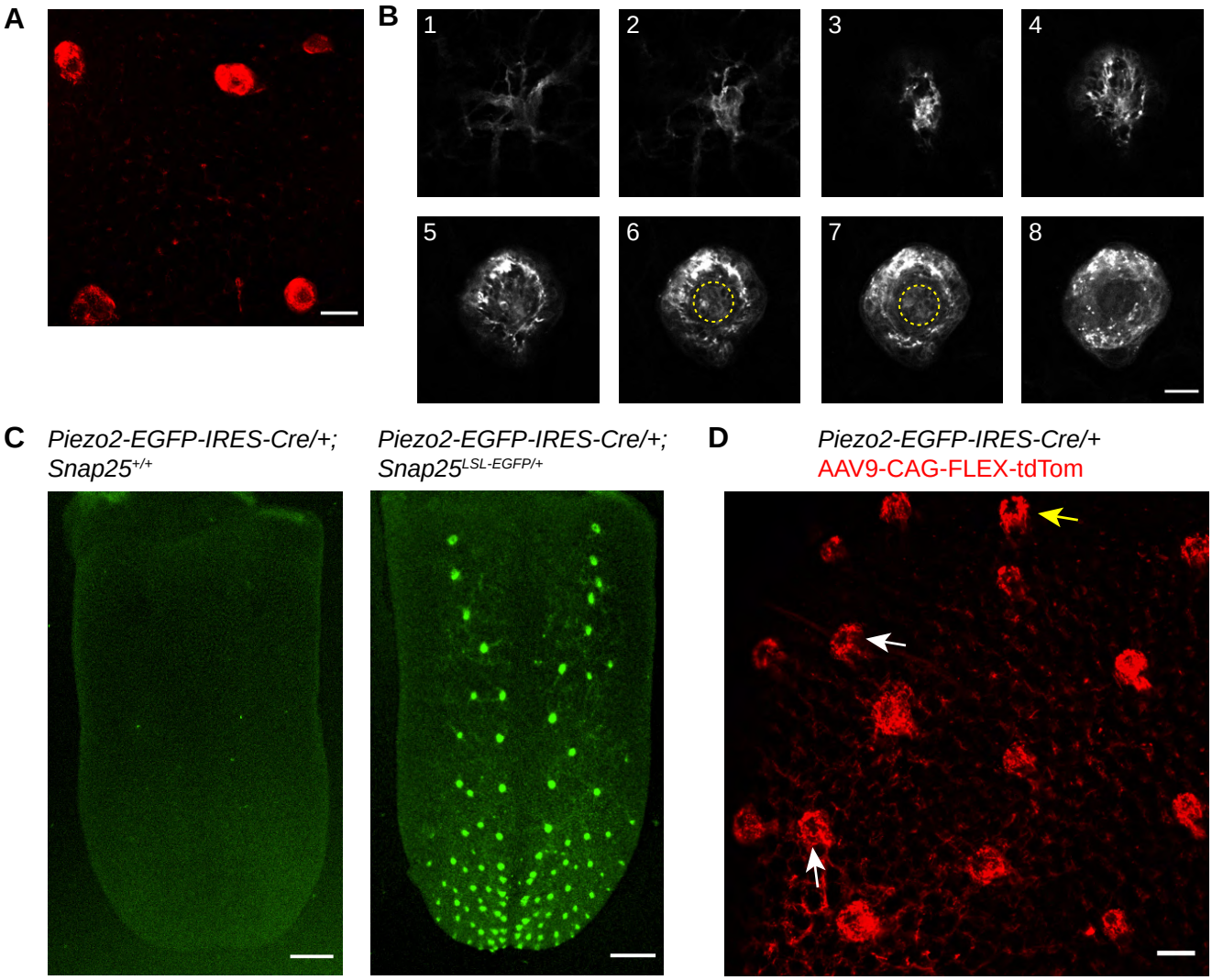

Figure 3. Similar to Piezo2+ afferents, trigeminal afferents innervate the extragemmal region of fungiform papillae and exhibit a ring-like termination pattern surrounding the taste pore

(A) An unsaturated maximum intensity projection of the confocal z-stack in Figure 2B showing the ring-like innervation pattern of DiI-labeled trigeminal afferents in fungiform papillae. Scale bar: 100 µm.

(B) Optical sections of DiI-labeled trigeminal axons in a fungiform papilla from a top-down view. The sections are labeled in an order from the deeper connective tissue (section 1) to the apical epithelium (section 8). Taste bud regions are circled in yellow dash lines in sections 6 and 7. Scale bar: 25 µm.

(C) Dorsal view of the tongue in a *Piezo2-EGFP-IRES-Cre/+;Snap25*$^{LSL\text{-}EGFP/+}$ mouse and its *Piezo2-EGFP-IRES-Cre/+; Snap25*$^{+/+}$ littermate. Scale bar: 500 µm.

(D) In *Piezo2-EGFP-IRES-Cre/+* mice injected with AAV9-CAG-FLEX-tdTom, tdTomato-labeled Piezo2 expressing afferents were found to innervate both fungiform and filiform papillae. The Piezo2^{+} nerve terminals also innervated the extragemmal region of an obliquely sectioned fungiform papilla (yellow arrow) and formed a ring-like innervation pattern in an *en face* sectioned fungiform papilla (white arrows). Scale bar: 100 µm.

A
Tongue
Plp1-EGFP/+ mouse
Glabrous skin
DAPI
EGFP
S100β
NFH
Merge
B
Filiform
Fungiform
Pirt Cre/+;R26 LSL-tdTom/+;Plp1-EGFP/+
DAPI
EGFP
tdTom
Merge
C
Filiform
Fungiform
Vglut2 Cre/+;R26 LSL-tdTom/+;Plp1-EGFP/+
D
Filiform
Fungiform
Split Cre/+;R26 LSL-tdTom/+;Plp1-EGFP/+

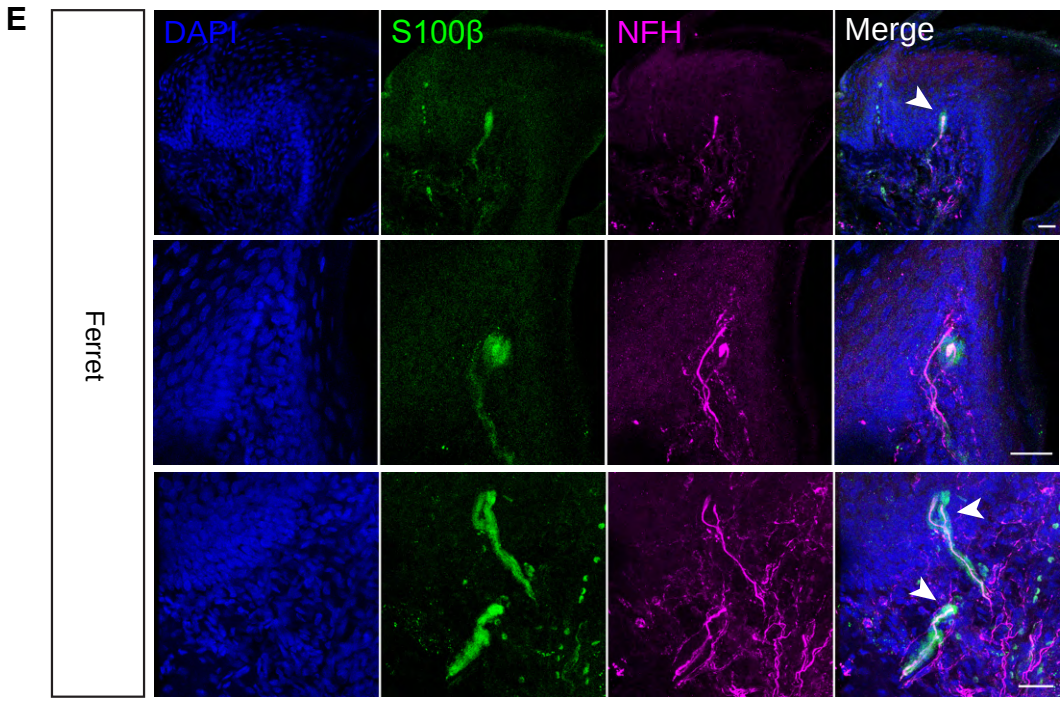

Figure 4. Mouse filiform papillae are innervated by NFH+ myelinated free nerve endings, while ferret filiform papillae contain corpuscular organs resembling end bulbs of Krause

(A) In the tongue of *Plp1-EGFP/+* mice, no corpuscular end organs but only myelinated free nerve endings can be identified in the connective tissue core of filiform papillae (top), compared to the glabrous skin, where Meissner corpuscles can be found in the dermal papillae (bottom). DAPI: cell nucleus. EGFP and S100β: (terminal) Schwann cells. NFH: myelinated nerve fibers. Asterisks: cell bodies of Schwann cells. Arrows: cell processes or myelin from Schwann cells. Scale bar: 20 µm.

(B) In *Pirt*$^{Cre/+}$*;R26*$^{LSL\text{-}tdTom/+}$*;Plp1-EGFP/+* mice, tdTom-labeled, myelinated afferents that colocalized with EGFP can be seen in both filiform and fungiform papillae. Taste bud cells in and around fungiform papillae were also labeled by *Pirt*^{Cre} (asterisks). The myelin was lost at the nerve terminal in myelinated afferents (triangles). *Pirt*^{Cre} also labeled unmyelinated afferents (thin arrows).

(C) In *Vglut2*$^{Cre/+}$*;R26*$^{LSL\text{-}tdTom/+}$*;Plp1-EGFP/+* mice, tdTom-labeled, myelinated afferents that colocalized with EGFP can be seen in both filiform and fungiform papillae. Muscles were also labeled by *Vglut2*^{Cre} (asterisks). In fungiform papillae, *Vglut2*^{Cre} labeled intragemmal (arrowhead) and extragemmal (thick arrows) afferents, both of which were not myelinated at the nerve terminals. *Vglut2*^{Cre} also labeled unmyelinated afferents (thin arrows).

(D) *Split*^{Cre} labeled unmyelinated afferents in both filiform and fungiform papillae (arrows). Scale bars in **(B-D)**: 20 µm.

(E) In ferret tongue, corpuscular end organs with cylindrical (top, bottom) or globular (middle) shapes resembling end bulbs of Krause can be seen in the connective tissue core or the basal layer of epithelium in filiform papillae, usually with blunt, enlarged nerve endings (arrowheads). The structure of filiform papillae is more complex in ferrets, as there can be more than one connective tissue papillae inside a single fungiform papilla (top). Scale bar: 25 µm.

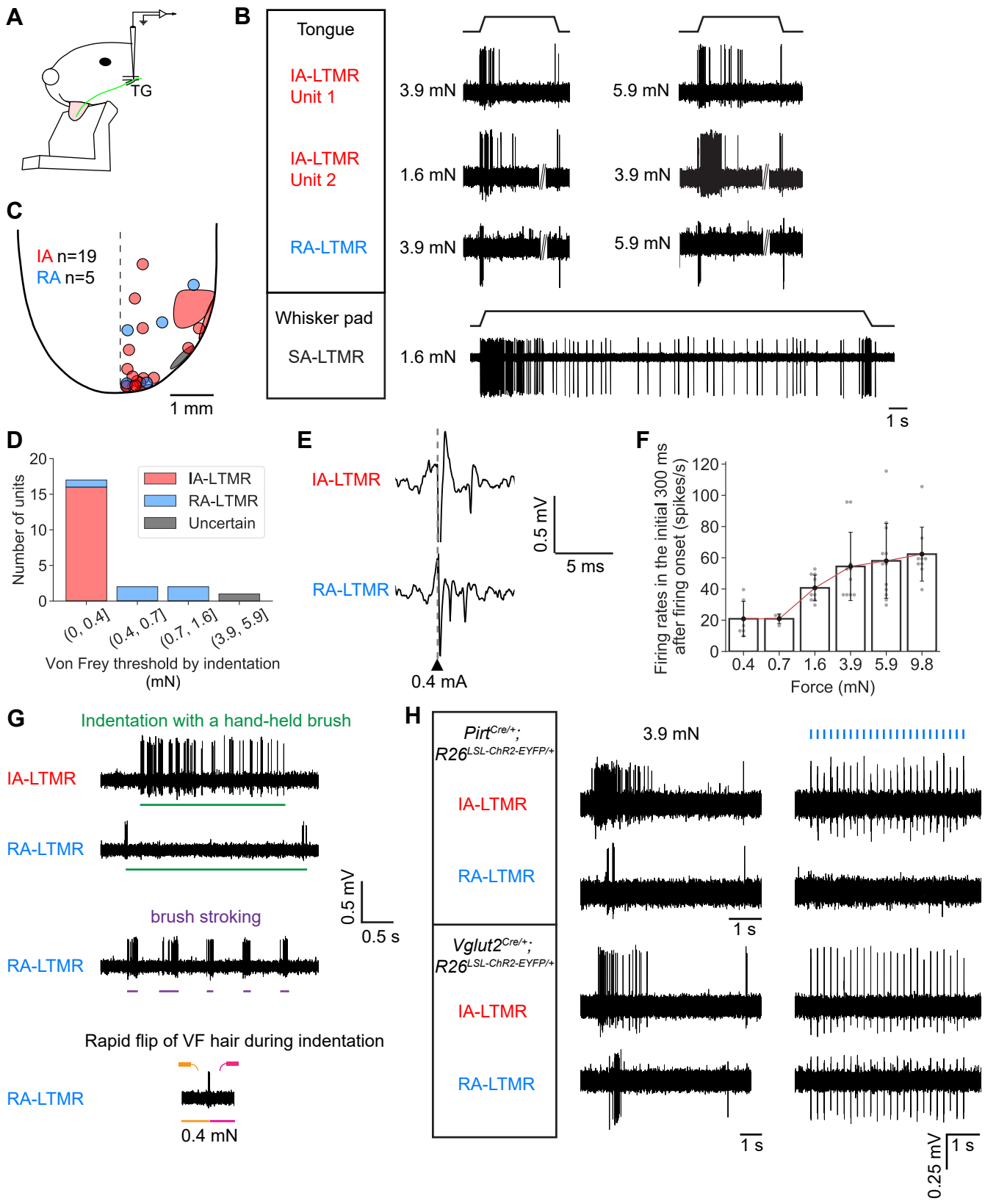
A
TG
B
Tongue
IA-LTMR Unit 1
IA-LTMR Unit 2
RA-LTMR
Whisker pad
SA-LTMR
3.9 mN
5.9 mN
1.6 mN
3.9 mN
3.9 mN
5.9 mN
1.6 mN
1 s
C
IA n=19
RA n=5
1 mm
D
Number of units
IA-LTMR
RA-LTMR
Uncertain
(0, 0.4]
(0.4, 0.7]
(0.7, 1.6]
(3.9, 5.9]
Von Frey threshold by indentation (mN)
E
IA-LTMR
RA-LTMR
0.5 mV
5 ms
0.4 mA
F
Firing rates in the initial 300 ms after firing onset (spikes/s)
Force (mN)
0.4
0.7
1.6
3.9
5.9
9.8
G
Indentation with a hand-held brush
IA-LTMR
RA-LTMR
0.5 mV
0.5 s
brush stroking
RA-LTMR
Rapid flip of VF hair during indentation
RA-LTMR
0.4 mN
H
Pirt Cre/+; R26 LSL-ChR2-EYFP/+
IA-LTMR
RA-LTMR
Vglut2 Cre/+; R26 LSL-ChR2-EYFP/+
IA-LTMR
RA-LTMR
3.9 mN
1 s
1 s
0.25 mV
1 s

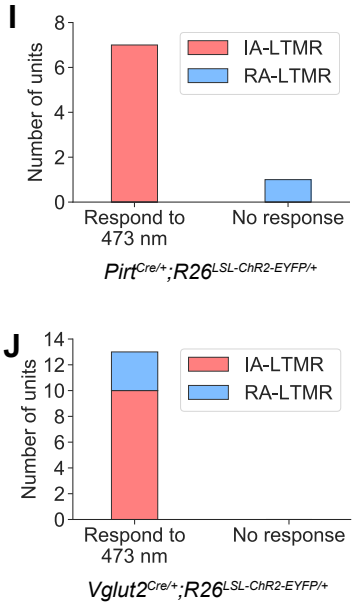

Figure 5. Single-unit recordings reveal two types of lingual LTMRs with distinct tactile response properties and conduction velocities in the A-fiber range

(A) Schematic of the single-unit recording setup. Green: lingual nerve.

(B) Neural activities of single lingual LTMR units recorded in TG in response to tactile indentation exerted at their receptive fields at the tongue surface. Neural traces with no spikes were cropped in order to make the onsets and offsets of indentation aligned for each column. An example SA-LTMR innervating the whisker pad was included as a comparison.

(C) The receptive fields of lingual LTMRs mapped by von Frey hairs (n = 25 from 19 mice; 19 IA-LTMRs, 5 RA-LTMRs and 1 unit that cannot be categorized into IA or RA).

(D) The von Frey indentation threshold for lingual LTMRs (n = 22 from 16 mice; 16 IA-LTMRs, 5 RA-LTMRs and 1 unit that cannot be categorized into IA or RA).

(E) Example neural traces in conduction velocity tests. The gray dashed line indicates the timepoint when a 0.4 mA electrical pulse was given to the unit's receptive field.

(F) The firing rates of an example IA-LTMR in the initial 300 ms after firing onset during von Frey indentation (average and standard deviation).

(G) The activities of lingual LTMRs in response to various tactile stimuli. IA-LTMRs were sensitive to slight vertical force changes and fired constantly when indented with a hand-held brush (non-static force). RA-LTMRs were sensitive to brush stroking and rapid changes of von Frey buckling direction, even when the von Frey hair used were below their indentation thresholds (the bottom row shows a RA-LTMR with a von Frey threshold higher than 0.4 mN).

(H) Neural activities of single lingual LTMR units recorded in TG in response to von Frey indentation and 473 nm light stimulation at their receptive fields in *Pirt*$^{Cre/+}$;*R26*$^{LSL\text{-}ChR2\text{-}EYFP/+}$ and *Vglut2*$^{Cre/+}$;*R26*$^{LSL\text{-}ChR2\text{-}EYFP/+}$ mice. Blue bars: 10 ms-duration 473 nm light pulses shone at 5 Hz.

(I-J) Number of lingual LTMR units that can or cannot be activated by 473 nm light stimulation from 3 *Pirt*$^{Cre/+}$; *R26*$^{LSL\text{-}ChR2\text{-}EYFP/+}$ mice and 8 *Vglut2*$^{Cre/+}$;*R26*$^{LSL\text{-}ChR2\text{-}EYFP/+}$ mice.

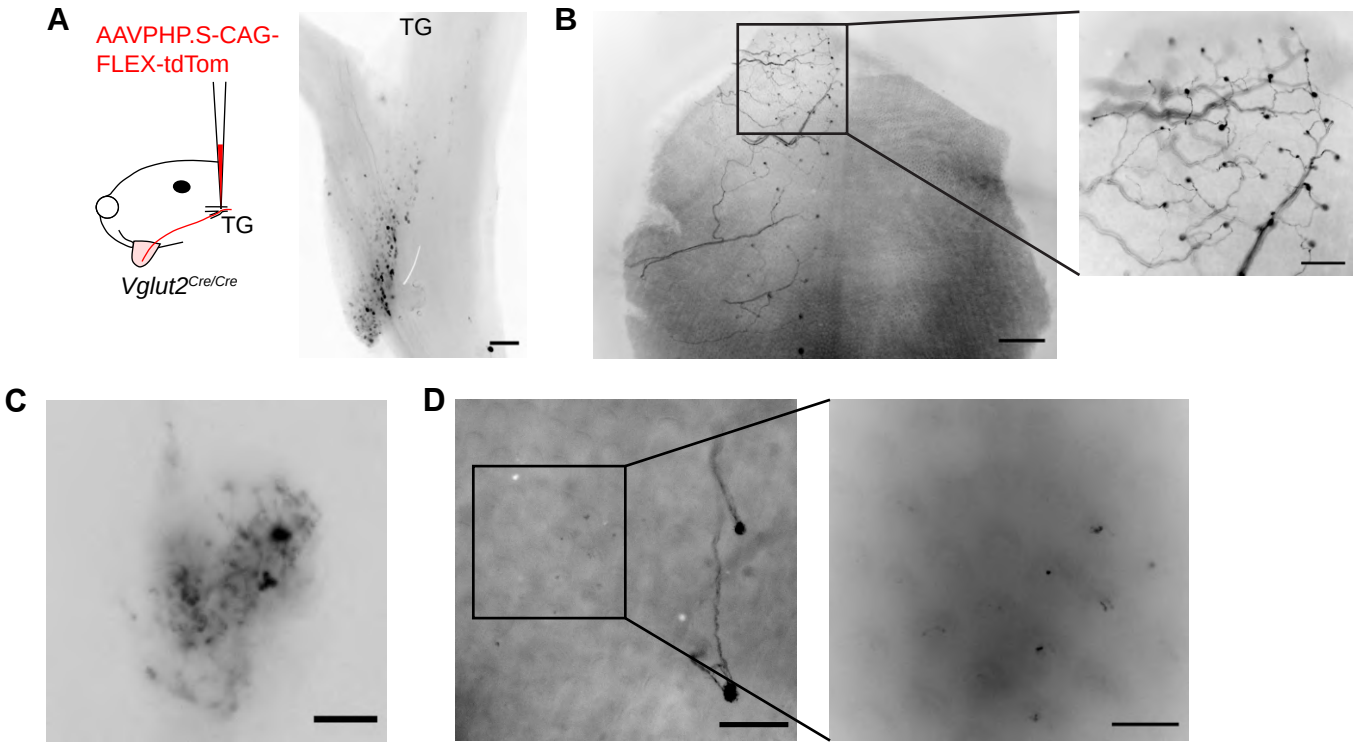

Figure 6. Lingual neurons that terminate in different types of papillae form distinct terminal fields
(A) Left: schematic of unilateral viral injection into the mandibular branch of the left TG in *Vglut2*$^{Cre/Cre}$ mice. Right: neurons at the mandibular branch of the left TG were labeled by tdTom driven by *Vglut2*^{Cre} at 3 weeks after viral injection. Scale bar: 300 µm.
(B) tdTom-labeled trigeminal axons at the tongue surface. Only the left side of the tongue was labeled after unilateral viral injection. Scale bar: 800 µm. Inset: A zoomed-in view of the tip of the tongue showing many fungiform papillae strongly labeled by tdTom. Scale bar: 300 µm.
(C) Tens of nerve terminals were labeled by tdTom inside a single fungiform papilla. Scale bar: 20 µm.
(D) Some filiform papillae localized in a cluster were labeled by tdTom, but weakly, compared to fungiform papillae. Scale bar: 200 µm. Inset: a zoomed-in view of the nerve terminals labeled by tdTom in the filiform papilla cluster. Scale bar: 100 µm.

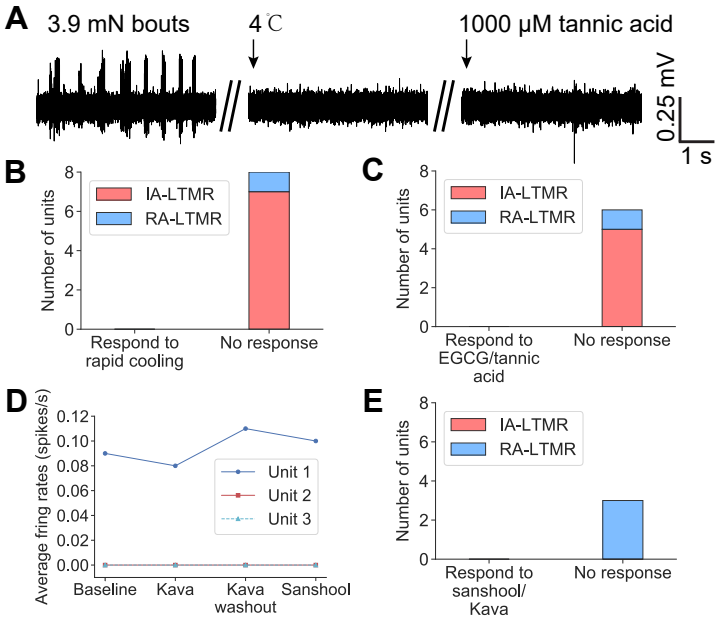

Figure 7. Lingual LTMRs are insensitive to rapid cooling or chemicals that can induce astringent or numbing sensations

(A) Neural activities of single lingual LTMR units recorded in TG in response to von Frey indentation, rapid cooling or chemicals that can induce astringent or numbing sensations (only tannic acid at the highest concentration is shown).

(B) Lingual LTMRs including both IA and RA did not respond to rapid cooling (n = 7 and 1 for IA and RA, respectively, from 6 mice).

(C) Lingual LTMRs including both IA and RA did not respond to EGCG/tannic acid in a series of concentrations (n = 5 and 1 for IA and RA, respectively, from 5 mice).

(D) The average firing rates of RA-LTMRs before and during Kava/sanshool treatment (n = 3 from 2 mice).

(E) RA-LTMRs did not respond to sanshool or Kava (n = 3 from 2 mice).

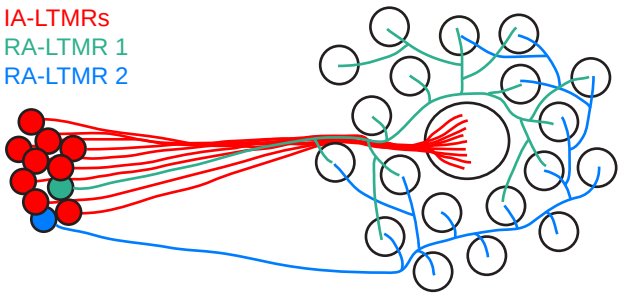

Figure 8. A working model of the organization of tactile innervation in the tongue
The schematic shows a hypothesis of how the lingual papillae at the tongue surface (blank circles at the right) could be innervated by lingual LTMRs in the TG (filled circles at the left). A single fungiform papilla (the big white circle) is innervated by many IA-LTMRs, while a single RA-LTMR innervates several adjacent filiform papillae (small white circles). The two colors of RA-LTMRs schematize two individual RA-LTMRs. Besides, a single filiform papilla may contain afferents from multiple LTMRs. The potential axonal branchings inside the papillae were not drawn.

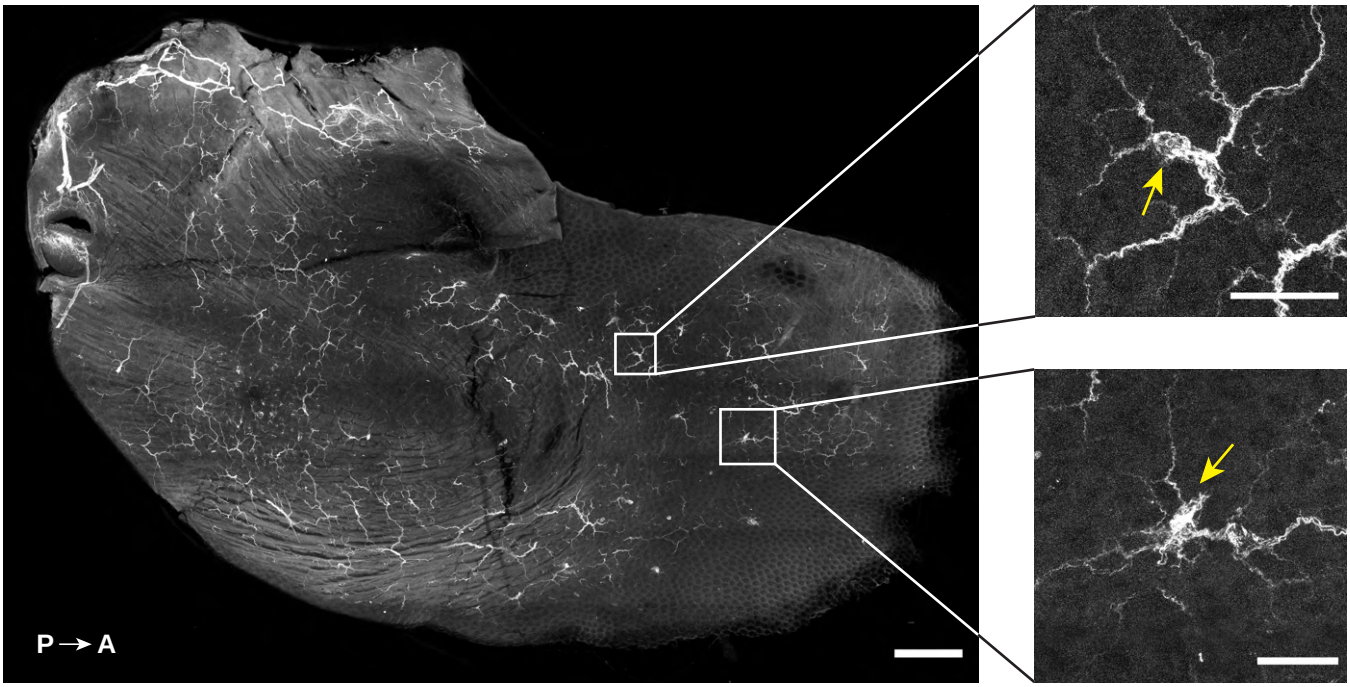

Figure S1. **NFH⁺ neural afferents innervate the dorsal surface of the tongue**
Left: dorsal surface of the tongue treated by iDISCO tissue clearing and anti-NFH immunostaining.
The tip of the tongue was cut off by sectioning and points towards the right side of the image. NFH⁺ neural afferents innervate both anterior and posterior regions of the tongue dorsal surface, and were seen to be enriched in fungiform papillae (yellow arrows) as shown in insets at the right. The arrows point at fungiform papillae. Scale bars: 500 µm at the left and 100 µm for insets.

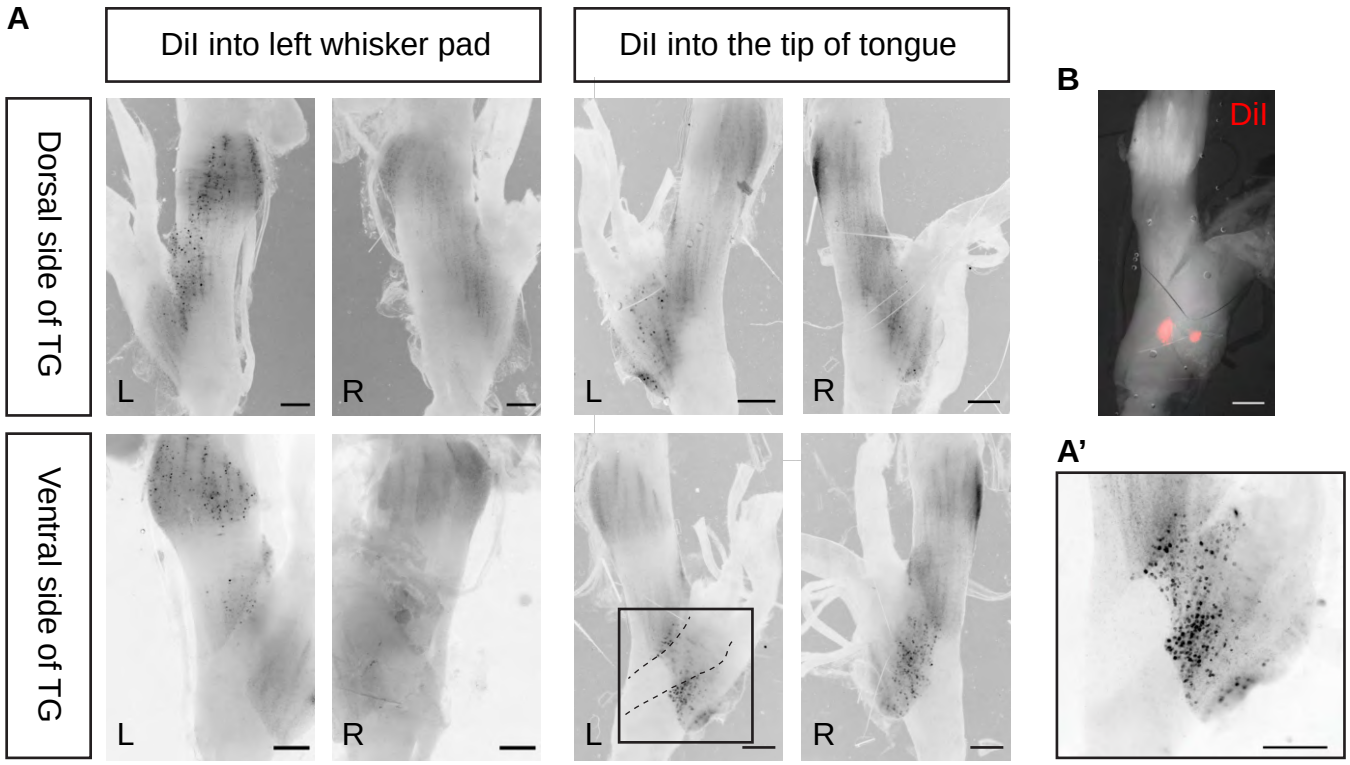

Figure S2. The somatotopic organization of trigeminal ganglion neurons innervating the whisker pad or the tip of the tongue

(A) Whole-mount imaging of the dorsal or the ventral surface of TG after DiI tracing from the left whisker pad or the tip of the tongue. The trigeminal neurons innervating the left whisker pad were located in the maxillary branch of the left TG, whereas those innervating the tip of the tongue were in the mandibular branch of TG and were most abundant at the ventral side of TG. The dashed line marks the boundary of a nerve trunk running through the ventral surface of TG. L: the left TG; R: the right TG. Scale bar: 500 µm.

(A') A zoomed-in view of the inset in **(A)** after dissecting the nerve trunk to reveal the cell bodies underneath. Scale bar: 500 µm.

(B) The ventral view of the left TG showing location of recorded lingual LTMRs marked by a DiI-coated tungsten electrode. Scale bar: 500 µm.

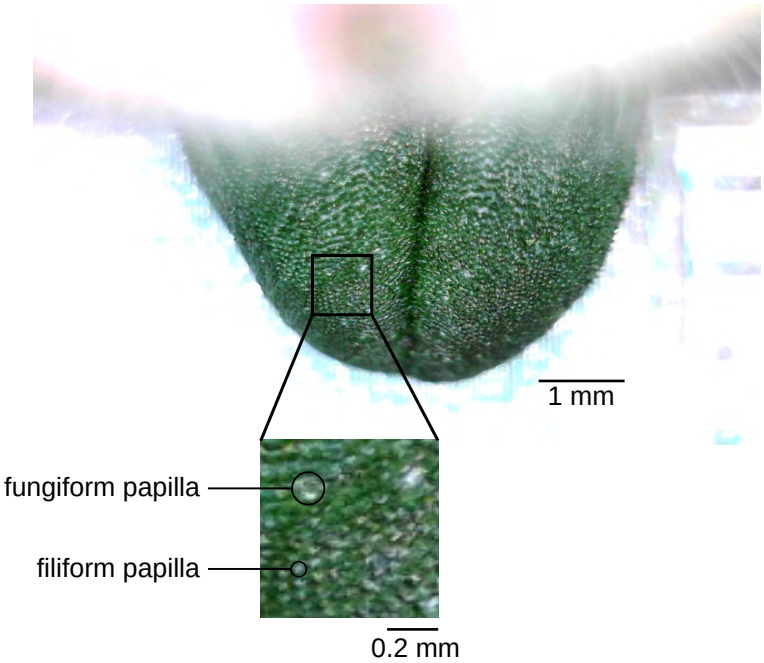

Figure S3. Fungiform and filiform papillae on a mouse tongue stained by a green food color